Published in final edited form as:

Neuroimage. 2020 September ; 218: 117001. doi:10.1016/j.neuroimage.2020.117001.

Functional connectivity of EEG is subject-specific, associated with phenotype, and different from fMRI

Maximilian Nentwich[a], **Lei Ai**[b], **Jens Madsen**[a], **Qawi K. Telesford**[c], **Stefan Haufe**[d,e], **Michael P. Milham**[b,c], **Lucas C. Parra**[a,*]

[a]Department of Biomedical Engineering, The City College of New York, New York, NY, USA

[b]Center for the Developing Brain, The Child Mind Institute, New York, NY, USA

[c]Center for Biomedical Imaging and Neuromodulation, The Nathan Kline Institute for Psychiatric Research, Orangeburg, NY, USA

[d]Berlin Center for Advanced Neuroimaging, Charité – Universitatsmedizin Berlin, Berlin, Germany

[e]Bernstein Center for Computational Neuroscience Berlin, Berlin, Germany

Abstract

A variety of psychiatric, behavioral and cognitive phenotypes have been linked to brain "functional connectivity" – the pattern of correlation observed between different brain regions. Most commonly assessed using functional magnetic resonance imaging (fMRI), here, we investigate the connectivity-phenotype associations with functional connectivity measured with electroencephalography (EEG), using phase-coupling. We analyzed data from the publicly available Healthy Brain Network Biobank. This database compiles a growing sample of children and adolescents, currently encompassing 1657 individuals. Among a variety of assessment instruments we focus on ten phenotypic and additional demographic measures that capture most of the variance in this sample. The largest effect sizes are found for age and sex for both fMRI and EEG. We replicate previous findings of an association of Intelligence Quotient (IQ) and Attention

*Corresponding author. parra@ccny.cuny.edu (L.C. Parra).

CRediT authorship contribution statement

Maximilian Nentwich: Conceptualization, Methodology, Software, Formal analysis, Data curation, Writing - original draft, Writing - review & editing, Visualization. **Lei Ai:** Software, Data curation, Writing -original draft. **Jens Madsen:** Software, Data curation. **Qawi K. Telesford:** Software, Data curation, Writing - review & editing. **Stefan Haufe:** Methodology, Software, Validation, Writing - review & editing. **Michael P. Milham:** Methodology, Resources, Writing - review & editing, Supervision, Funding acquisition. **Lucas C. Parra:** Conceptualization, Methodology, Software, Resources, Writing - review & editing, Supervision, Project administration, Funding acquisition.

Ethics statement

The IRB for the HBN data was approved by the Chesapeake Institutional Review Board (https://www.chesapeakeirb.com/). Written informed consent was obtained from all participants above 18 years, prior to conducting research. In the case of participants below 18 years of age, written assent obtained. Additionally written consent was obtained from their legal guardians (Alexander et al., 2017). Neuroimaging data from the HBN Biobank is publicly available and de-identified. The corresponding phenotypic data is available under a data usage agreement (http://fcon_1000.projects.nitrc.org/indi/cmi_healthy_brain_network/File/CMI_Biobank_DUA.pdf) to ensure privacy, confidentiality and security of the data.

Declaration of competing interest

The authors declare no conflict of interest.

Appendix A. Supplementary data

Supplementary data to this article can be found online at https://doi.org/10.1016/j.neuroimage.2020.117001.

Deficit Hyperactivity Disorder (ADHD) with the pattern of fMRI functional connectivity. We also find an association with socioeconomic status, anxiety and the Child Behavior Checklist Score. For EEG we find a significant connectivity-phenotype relationship with IQ. The actual spatial patterns of functional connectivity are quite different between fMRI and source-space EEG. However, within EEG we observe clusters of functional connectivity that are consistent across frequency bands. Additionally we analyzed reproducibility of functional connectivity. We compare connectivity obtained with different tasks, including resting state, a video and a visual flicker task. For both EEG and fMRI the variation between tasks was smaller than the variability observed between subjects. We also found an increase of reliability with increasing frequency of the EEG, and increased sampling duration. We conclude that, while the patterns of functional connectivity are distinct between fMRI and phase-coupling of EEG, they are nonetheless similar in their robustness to the task, and similar in that idiosyncratic patterns of connectivity predict individual phenotypes.

Keywords

Electroencephalography (EEG); Functional magnetic resonance imaging (fMRI); Functional connectivity; Imaginary coherence; Brain–behavior relationships; Reliability

1. Introduction

The term “functional connectivity” (FC) in neuroscience refers to various measures of how neural activity in one brain area relates to activity in another. Although conceptually simple, FC has emerged as a mainstream approach in the fMRI community for delineating large-scale brain “networks” (i.e. groups of spatially segregated brain areas which fluctuate in unison), which exhibit a high degree of reproducibility across laboratories and methods. Importantly, studies have found that with sufficient data, functional networks can be reliably and reproducibly identified in the FC during rest (Elliott et al., 2019; Noble et al., 2019; O’Connor et al., 2017); and that variations appear to be associated with neuropsychiatric developmental variables and disorders (Finn et al., 2015; Gao et al., 2019; Rosenberg et al., 2016; Shehzad et al., 2014; Smith et al., 2015; Takagi et al., 2019). Specifically, patterns of FC have been associated with IQ and ADHD (Shehzad et al., 2014), fluid intelligence (Finn et al., 2015), attention (Rosenberg et al., 2016), and lifestyle, demographic and psychometric variables (Smith et al., 2015). Recognizing the successes of FC studies in fMRI, an obvious question that arises is whether FC methods have the same potential to become mainstream tools for other modalities, such as EEG.

For fMRI, FC is commonly measured as the Pearson’s correlation of the time courses between different brain areas (Biswal et al., 1995; Fox and Raichle, 2007). Recently, more sophisticated methods for the estimation of FC in fMRI have been developed to extend the traditional approach on FC (Bullmore and Sporns, 2009; Bullmore and Bassett, 2011; Smith et al., 2011). These attempt to capture different time scales (Bullmore et al., 2004), reduce common sources of variance (Salvador et al., 2005), capture delayed correlations (Kitzbichler et al., 2009), or capture causation (Reid et al., 2019). Some of them have also been linked to phenotypic variables such as age (Meunier et al., 2009; Mowinckel et al.,

2012), fluid intelligence (Ezaki et al., 2019), and schizophrenia (Fornito et al., 2012), and different methods for correlating with phenotype have been benchmarked (Dadi et al., 2019). However, the vast majority of work in this regard is based on Pearson's correlation, which we will use in the current analysis.

For EEG and MEG, several FC measures have been devised focusing either on the amplitude or the phase of oscillatory activity in different frequency bands (Bastos and Schoffelen, 2016; Colclough et al., 2016; Demuru et al., 2020; Marzetti et al., 2019; Nolte et al., 2004; Palva et al., 2018; Siems and Siegel, 2020; Wang et al., 2017). Correlation in amplitude, referred to as amplitude-coupling, results in FC patterns that can be similar to resting state FC in fMRI (Brookes et al., 2011a, 2011b; Hiltunen et al., 2014; Liu et al., 2018, 2017; Pasquale et al., 2010). A common concern with amplitude-coupling is that volume conduction results in spurious instantaneous correlations. Efforts to remove these artifacts yield amplitude-coupling patterns in MEG (Hipp and Siegel, 2015) and ECoG (Hacker et al., 2017) which are also similar to FC in fMRI. Indeed, one can find associations of amplitude-coupling patterns with age (Bathelt et al., 2013; Coquelet et al., 2017; Schäfer et al., 2014), or phenotypic variables such as autism (Kitzbichler et al., 2015) and schizophrenia (Brookes et al., 2016). Correlation of the voltage fluctuations with some time delay, referred to as phase-coupling, reduces the effects of volume conduction (Nolte et al., 2004). They have been used to characterize neuronal interactions (Fries, 2005), although more recent work shows that spurious interactions remain a concern (Palva et al., 2018b). There is some evidence that patterns of phase-coupling are similar to conventional FC in fMRI (Wirsich et al., 2017), but some components of these networks also appear to differ from fMRI (Wirsich et al., 2020). Phase-coupling has also been associated with some phenotypes such as age (He et al., 2019; Lavanga et al., 2018), sex (Fujimoto et al., 2016), and ADHD (Sudre et al., 2017). Amplitude and phase coupling measures capture fundamentally different aspects of FC (Nolte et al., 2019; Siems and Siegel, 2020), although amplitude coupling measures retain a dependence on phase (Palva et al., 2018). Specifically, phase and amplitude-coupling measures are most similar in short range connectivity and differ in long range connectivity which suggests different underlying neuronal mechanisms (Siems and Siegel, 2020). Here we focus on a phase-coupling measure that is insensitive to volume conduction (Nolte et al., 2004), namely, the imaginary part of coherency (iCOH), which has been extensively validated (Mahjoory et al., 2017; Nolte et al., 2019; Wang et al., 2014).

There is also a growing interest in FC evaluated not just during rest but during task performance, and in particular during viewing of natural stimuli such as video (Elliott et al., 2019; O'Connor et al., 2017; Schmälzle et al., 2017; Vanderwal et al., 2017). Therefore we here combine data from resting state as well as viewing of videos. For fMRI, FC patterns are highly correlated between tasks (Cole et al., 2014; Geerligs et al., 2015b; Vanderwal et al., 2017) and more similar within the same subject than between different subjects doing the same task (Finn et al., 2015; Laumann et al., 2015; O'Connor et al., 2017). This suggests that FC is a property of the individual, more so than a property of the task. Together with its correlation to phenotypic information, this suggests that FC can be used as a diagnostic metric to assess individuals. Here we explore these issues of robustness, individuality, and correlation to phenotype for the phase-coupling of EEG, and compare this to fMRI in a large cohort of children and adolescents.

We find that phase-coupling of EEG clusters into distinct FC networks that are consistent across frequency bands, hemispheres, and tasks but differ across subjects, making them predictive of individual demographic and phenotypic variables. While this parallels findings with FC in fMRI, the actual networks are genuinely different from fMRI networks, providing a potential new direction for future FC research.

2. Results

We analyzed data from children and adolescents (5–21 years old) collected by the Healthy Brain Network (HBN) (Alexander et al., 2017). From the total of 1657 participants (up to data release 6), clean EEG data was available from 1330 participants and fMRI data from 766 participants (Fig. 1B and Section 5.1). fMRI and EEG recordings were available during rest and during passive viewing of naturalistic narrative videos (see Section 5.1). Additional EEG data was available during visual presentation of flashing gratings designed to measure steady state visual evoked potentials (Vanegas et al., 2015) (see Section 5.1).

fMRI data was preprocessed as reported previously (Craddock et al., 2013) (see Section 5.7). Cortical fMRI activity was averaged across voxels belonging to each area of the Schaefer atlas (N = 200 areas) (Schaefer et al., 2018) and FC was calculated as the Pearson's correlation coefficients between these areas. After automated preprocessing (see Sections 5.3 to 5.5), EEG activity was source-localized to the Freesurfer fsaverage surface template with 2003 voxels using the eLORETA algorithm in cartesian x,y,z directions (Pascual-Marqui, 2007). The source-space time series from each area of the Schaefer parcellation (Schaefer et al., 2018) were aggregated using principal component analysis (PCA). FC between each area of the Schaefer atlas was then calculated using the imaginary part of coherency (iCOH) (Nolte et al., 2004) on the strongest PCA components (see Section 5.6). The iCOH method reduces the contribution of volume conduction to FC compared to standard coherence (absolute value of complex coherency). iCOH is computed for frequency bins of 0.5 Hz resolution up to the Nyquist frequency (62.5 Hz). Delta, theta, alpha and beta band FC was obtained by averaging across respective frequency bins (see Section 5.8). Broadband FC averages the entire range from 0.5 to 30 Hz.

2.1. FC of EEG clusters into distinct brain networks, consistently across frequency bands, but differently from FC of fMRI

The iCOH connectivity matrices in EEG source space can be organized by clusters of voxels with similar connectivity patterns (Fig. 2A, top). Here we used the connectivity matrix averaged over all subjects and cluster this following the same procedure as in previous work for fMRI (Yeo et al., 2011) (see Section 5.9). The clustering of the FC obtained using the HBN fMRI data is very similar to that of Yeo et al. (Fig. A1). When the same clustering method is applied to the FC of EEG we obtain consistent clusters across frequency bands, but they differ substantially from the clusters in the FC of the fMRI (Fig. 2B). We note that the spatial arrangement of the clusters in EEG are extended in space and not necessarily contiguous (Fig. 2A, bottom). They are also fairly consistent between hemispheres, despite clustering hemispheres separately from one another (Fig. 2A, bottom). This rules out spatial proximity as the primary cause for this consistent clustering. In fact, note that the

connectivity within clusters is lower than between clusters (Fig. 2A, top). This is the result of the iCOH method, which is designed to remove instantaneous correlations, so that all correlations imply a time delay.

2.2. FC of fMRI is different from the FC of EEG

Given the distinct clustering it seems that the FC of EEG and fMRI are genuinely different. To quantify this we measure the similarity of FC between EEG and fMRI on individual subjects. For each subject we computed the Pearson's correlation coefficient between the EEG and fMRI FC matrix (vectorized), and then averaged these correlations over subjects. The mean correlation is low and not significant in any of the frequency bands. Significance was determined by shuffling the subject labels and computing the same average correlation coefficient. (delta, r = 0.052, p = 0.19; theta, r = 0.078, p = 0.58; alpha, r = 0.103, p = 0.45; beta, r = 0.102, p = 0.89, broadband, r = 0.12, p = 0.75). We confirm these findings using three other measures of similarity, image intraclass correlation coefficient (I2C2) (Shou et al., 2013), Multiscale Graph Correlation (MGC) algorithm (Shen et al., 2018; Vogelsteinetal., 2019) and geodesic distance (Venkatesh etal., 2020) (see Supplement). Given these results and the distinct clusters of connectivity shown in Fig. 2 we conclude that the patterns of FC in EEG and fMRI are different in all frequency bands measured.

2.3. FC is similar across tasks, for both fMRI and EEG

We wanted to establish how similar FC patterns are across the different tasks (resting state, video viewing, flashing gratings). To this end, we measured the similarity of FC between different tasks (similarity is measured as Pearson's correlation across edges of the FC matrix). We contrast this with the similarity of FC between different subjects (Fig. 3A). Evidently FC are significantly better reproduced across tasks than across subjects. This is true for fMRI, replicating known results (O'Connor et al., 2017), but also for EEG in all frequency bands tested. (Wilcoxon signed rank test: Delta: $\Delta_r = 0.061$, $p = 3.9*10^{-7}$, n = 50; Theta: $\Delta_r = 0.13$, $p = 9.5*10^{-9}$, n = 50; Alpha: $\Delta_r = 0.22$, $p = 7.6*10^{-10}$, n = 50; Beta: $\Delta_r = 0.22$, $p = 7.6*10^{-10}$, n = 50; Broadband: $\Delta_r = 0.24$, $p = 8*10^{-10}$, n = 50; fMRI: $\Delta_r = 0.16$, $p = 1.6*10^{-59}$, n = 355; Δ_r: median difference of Pearson's correlation coefficient. Given the strength of these effects this analysis was limited to 50 subjects that completed all EEG recordings and whose data is of good quality.)

This consistency of the FC across tasks (relative to variability observed across subjects) can be quantified in a single metric, namely the inter-class correlation (ICC) (McGraw and Wong, 1996; Shrout and Fleiss, 1979). An ICC value of 1 would indicate perfect consistency of FC between tasks, whereas an ICC of 0 would indicate perfect consistency of FC between subjects and not tasks (see Section 5.13). For EEG we measured reliability of FC across tasks, and did this separately for different frequency bands. Reliability increases from low to high frequency bands (Fig. 3B). In the beta band tasks are most consistent within the visual network, while in all other bands tasks are least consistent within the visual network (Fig. A2). For fMRI we measured reliability across sessions to determine if longer segments of data lead to more stable FC matrices. We do this separately for resting state (2C) and video viewing (2D). As expected we see that longer data segments increase reliability of the FC matrix (O'Connor et al., 2017). Therefore, in all further analysis we compute FC using

combined data from rest and task conditions, as they appear to be stable within subjects and provide more robust estimates with longer data segments.

2.4. FC is associated with phenotypic and demographic information, for both fMRI and EEG

Of the available phenotypic data we selected a subset of 10 assessment instruments, which were available for most subjects and which contributed most strongly to shared variance in the population (Fig. 4A). Specifically, these 10 had the strongest component weights in a principal component analysis and the assessments questionnaires had been completed by at least 50% of participants (see Section 5.2). We also included age and sex as two important demographic variables that are well known to affect neuroimaging results (Biswal et al., 2010; Geerligs et al., 2015a; Ingalhalikar et al., 2014; Kilpatrick et al., 2006; Tomasi and Volkow, 2012). When referring to “phenotype” in the following we implicitly also refer to these two demographic variables. To establish a link between connectivity patterns and phenotype we used multivariate distance matrix regression (MDMR) (Mcardle and Anderson, 2001; Shehzad et al., 2014) (see Section 5.11). In essence, MDMR measures whether individuals with similar patterns of connectivity also have similar scores on a given phenotypic assessment instrument. Similarity of connectivity is measured by Pearson’s correlation across edges of the FC matrix. Pearson’s correlation is not affected by differences in means and measures the similarity of patterns of connectivity. Thus, overall strength of FC is not used as a predictive factor. Analysis is performed separately for each of the 10 phenotypic assessment instrument, in addition to the two demographic variables age and sex.

2.5. fMRI FC - phenotype associations

The MDMR analysis reveals a significant association between fMRI FC for a number of the measures tested (Fig. 4A). This includes age ($F = 8.71$, $p < 0.004$, N indicated in Fig. 4A), sex ($F = 1.87$, $p < 0.004$), the WISC IQ score ($F = 1.72$, $p < 0.004$), the CBCL score for multiple disorders ($F = 1.42$, $p = 0.0072$), the Barratt SES score ($F = 1.36$, $p = 0.006$) and SWAN ADHD score ($F = 1.32$, $p = 0.01$). An additional weak correlation is found between FC and the SCARED Anxiety score ($F = 1.28$, $p = 0.031$). P-values are FDR corrected. To avoid confounds with age and sex we regressed out a possible linear effects of age and categorical effect of sex from the other phenotypic and demographic variables prior to MDMR (see Fig. A4). The MDMR analysis reported above was done on FC combining resting state and video viewing. Notably, connectivity-phenotype relationships are found for similar phenotypes even when MDMR is performed separately on FC of resting state and the video task (Fig. 4B), albeit with somewhat weaker effect sizes. See Table A1 for full statistics. This further validates our choice for combining data from multiple tasks to reduce noise and improve power for this analysis.

2.6. EEG source space FC - phenotype associations

FC of EEG computed in the source space (see Sections 5.6 and Section 5.8) shows a strong association with age and sex in all frequency bands tested (Fig. 5A). Associations with the same 10 phenotypic variables only show a significant effect for IQ in the delta and beta bands (see Table A.2 for full statistics). In addition to regressing out the effects of sex and

age, we have regressed out head size as it is correlated with age and sex (Fig. A4). The highest connectivity-phenotype relationship is seen in the broadband FC, followed by the higher frequency bands, beta and alpha (Fig. 5A). This could be explained by the higher reliability of FC in the broadband signal and the beta band (Fig. 3A), consistent with prior literature (Hipp and Siegel, 2015; Siems and Siegel, 2020).

The associations found with EEG coincide with those of fMRI connectivity. The analysis has also been conducted for different age groups (Fig. A6). While the specific statistics are somewhat different, the results are largely the same in the two age groups tested (5–9 years and 10–21 years). As with fMRI, the analysis here was done by combining EEG recordings from resting state and task performance. When we split the data by task (rest, video, flicker) the results do not differ much (Fig. 5B), again, consistent with the robustness of FC across tasks (Fig. 3). We find similar results when we perform the FC-phenotype analysis using alternative methods (see Fig. A7).

2.7. EEG sensor space FC - phenotype associations

Functional connectivity computed directly on sensor-space EEG data shows relationships to similar phenotypes as source-space FC (Fig. 5C). However, the effect size is larger in source space. Additionally, it has been shown that spatial patterns of FC in sensor space depend on the selection of the reference channel (Mahjoory et al., 2017). Therefore, we here focus on analyzing the spatial patterns of connectivity-phenotype relationships in source space.

2.8. Spatial patterns of FC-phenotype associations

Thus far we have associated phenotypes with a global pattern of FC. To determine which brain areas are specifically involved, we repeat the MDMR analysis separately for each brain region (based on the Schaefer atlas) (see Section 5.11). This indicates which nodes of the total brain network vary with phenotype (e.g. Fig. 6A). Additionally, we conducted the MDMR analysis for various resting-state networks (Yeo et al., 2011). This analysis reveals whether connectivity within or between networks drives the relationship to phenotypes (e.g. Fig. 6B). Both analyses were performed for the variables sex, age and IQ, which were linked to whole-brain FC for both fMRI and EEG. We can additionally establish the direction of the change by directly correlating connection strength with the phenotype (Figure A.9 and Figure A.10). However, the correlation of fMRI to age is weak and therefore very few nodes are significantly correlated to age after correction for multiple comparisons.

Sex effects: EEG connectivity differs with sex mostly for nodes in the occipital and parietal cortex (Fig. 6A). This is not a local property of the occipital visual network, but rather, it is the link of the visual network with the frontoparietal, default mode and attention networks that differ between the sexes (Fig. 6B). The strong effects of connectivity originating in the visual cortex can partly be explained by the relatively high reliability of connectivity in the visual cortex (Colclough et al., 2016). In the beta band median connectivity in most brain regions is larger in girls than in boys (Fig. A.9). This effect is a strong contrast to other frequency bands where the median connectivity is larger in boys. Interestingly, the absolute median difference of connectivity between boys and girls is largest in the visual cortex (Fig. A.9), while the patterns of connectivity are dissimilar within

the visual cortex (Fig. 6B). fMRI connectivity also differs with sex but the network nodes that are most affected appear to be quite different from the EEG connectivity. The strongest effects of the fMRI connectivity are seen in parietal and frontal lobes as well as the cingulate gyrus and are more focal than in EEG (Fig. 6A). In contrast to EEG connectivity, differences in fMRI connectivity within the ventral attention and default mode network are most strongly related to sex (Fig. 6B).

Age effects: EEG connectivity changes with age in all bands over broad cortical regions (Fig. 7A). Connectivity in the frontal lobe is related to age in all bands but the delta band. Age is related to connectivity between the visual and default mode, frontoparietal and ventral attention networks effects in delta and theta band (Fig. 7B). In the alpha and beta bands age differences correspond to differences in connectivity between the frontoparietal and default mode networks (Fig. 7B). In the beta band there is also a strong relationship of connectivity of the ventral attention network to other networks (Fig. 7B). Correlating age to connectivity in individual pairs of regions there is a drastic difference between bands. Delta, theta and beta band connectivity decrease with age and alpha connectivity increasing with age in most regions (Fig. A.10). fMRI connectivity is most strongly related to age in the parietal cortex, precuneus and posterior cingulate (Fig. 7A). This relationship is stronger and more focal than in EEG. The most distinct relationship between resting state networks and age is found within the ventral attention network and between the ventral attention and dorsal attention, frontoparietal and default mode networks (Fig. 7B). There is also a strong relationship of age to the connectivity within the visual, limbic, frontoparietal and default mode networks. Further, the relationship between age and the visual and dorsal attention network is strong. In terms of the correlation of age to connectivity in the ventral attention network, fMRI and EEG results are similar.

The effects of IQ - and SES - connectivity relationships are much weaker and thus harder to localize (Fig. 8). Given the general limitations localizing EEG sources these results should be regarded with care (Anzolin et al., 2019; Liu et al., 2018; Mahjoory et al., 2017). The relationship of fMRI connectivity to IQ is strongest in temporal and parietal lobes and is dominated by connectivity within the default mode network (Fig. 8).

3. Discussion

We have shown that phase-coupling measures of EEG cluster consistently across hemispheres and frequency bands. Notably, these clusters are different from clusters in fMRI (Yeo et al., 2011). Further, phase-coupling FC patterns can be seen as neural fingerprints that can distinguish subjects between each other and are consistent across tasks. Lastly, while FC patterns between EEG and fMRI are distinct, both are predictive of phenotypes such as age, sex and IQ.

3.1. Clustering of EEG FC

Clusters of EEG FC are extended in space and not always contiguous. This is important because clustering of FC could be confounded by “ghost interactions” (see Section 3.6). The spatially extended and distributed clusters suggest that “ghost interactions” are not the main effect driving clusters. Instead, clusters more probably represent functional units of EEG FC.

Phase-coupling FC is known to represent short range connectivity with less interhemispheric connections than amplitude coupling (Siems and Siegel, 2020). Thus the difference of clusters in EEG FC to fMRI could be partly driven by the measures of FC. Given the potential differences of phase-coupling and correlation, as well as physiological differences between EEG and fMRI, it is perhaps not surprising that clusters differ. This may warrant to use atlases specific to EEG FC in future studies.

3.2. Differences and similarities of FC in EEG and fMRI

The differences in FC between several EEG and fMRI measures have been investigated extensively (Colclough et al., 2016; Demuru et al., 2020; Siems and Siegel, 2020; Wirsich et al., 2020). Here wefind that the structure of the FC of EEG differs from that of fMRI (Fig. 2), at least for EEG “connectivity” measured using the method of imaginary coherence (iCOH). Nevertheless, the FC of fMRI and EEG behave similarly in several regards. In both modalities, FC are well preserved across tasks relative to the variability observed across subjects (Fig. 3). This has previously been established for fMRI (Finn et al., 2015; Laumann et al., 2015; O’Connor et al., 2017), and is found to be true also here for source-localized EEG at all frequency bands tested. For both modalities, FC is predictive of similar phenotypes and demographic variables (Figs. 4 and 5). Specifically, age, sex and IQ are all associated with whole-brain FC measured of either EEG or fMRI. In addition, we have found a relationship of fMRI FC to attention deficit disorder, anxiety, socio-economic status and an aggregate measure of behavioral and emotional problems. These connectivity-phenotype relationships are largely independent of the task subjects were performing. Thus, as with fMRI (Elliott et al., 2019; Noble et al., 2019; O’Connor et al., 2017) we recommend concatenating EEG data across different tasks to achieve more reliable measurements of FC and a stronger relationship to phenotypes. When we look at the details of the connectivity-phenotype association we do see some differences between the two modalities. EEG connectivity is more strongly related to sex than age (Fig. 4A) and vice versa for fMRI (Fig. 4A). Additionally, the spatial patterns of the connectivity-phenotype relationship are different in the two modalities (Figs. 6–8). This is perhaps not surprising given that the connectivity matrices themselves are quite different between modalities (Fig. 2).

Our results show that FC differs between EEG and fMRI, yet FC of both modalities correlate with phenotypes. This suggests that FC of EEG and fMRI contain complementary information consistent with previous literature (Wirsich et al., 2017). Both fMRI (Finn et al., 2015; Gao et al., 2019; Rosenberg et al., 2016; Shehzad et al., 2014; Smith et al., 2015; Takagi et al., 2019) and EEG FC (Bathelt et al., 2013; Brookes et al., 2016; Coquelet et al., 2017; Kitzbichler et al., 2009; Schäfer et al., 2014) have been related to phenotypes in separate studies. Therefore, both measures likely represent distinct aspects of neuronal activity that are behaviorally relevant.

3.3. Factors that may contribute to differences between EEG and fMRI

Factors that could explain these differences are the physiological origin of the two signals and the methods used to compute “connectivity”. Both factors vary drastically between modalities.

Both EEG and fMRI are thought to be related to post-synaptic potentials (Hall et al., 2014). Specifically, it has been shown that the fMRI BOLD signal is related to local field potentials in the gamma and high-frequency power (50–150 Hz and above 250 Hz respectively) (Conner et al., 2011; Haufe et al., 2018; Keller et al., 2013; Logothetis et al., 2001). Unfortunately, in scalp EEG the gamma band is largely contaminated by muscle activity (Muthukumaraswamy, 2013). This is especially problematic for recordings in children and adolescents, where movement artifacts are more frequent. Therefore we limit our analysis to the lower frequency bands, which do not correlate strongly with fMRI (Conner et al., 2011; Haufe et al., 2018; Keller et al., 2013; Logothetis et al., 2001).

An additional factor adding uncertainty to EEG-based FC estimation is that such connectivity analysis has proven to be dependent on how the sources of EEG activity are reconstructed (Liu et al., 2018, 2017; Mahjoory et al., 2017), or on the choice of reference electrode when working in the sensor space (Mahjoory et al., 2017). Even when working in the source space, there remains a dependence on the source reconstruction methods, head models and density of electrodes (Liu et al., 2018, 2017; Mahjoory et al., 2017). Future work may improve on the source reconstruction by using individualized head models based on the individual anatomical MRIs.

Amplitude-coupling in EEG shows a better correspondence to fMRI FC than what we found here for phase coupling (Hipp and Siegel, 2015). Phase-coupling measures are noisier than amplitude-coupling measures (Colclough et al., 2016). While our dataset is large enough to find a relationship of iOCH to phenotypes, the within subject correlations of FC is lower than reported for amplitude-coupling (Colclough et al., 2016) and fMRI (Fig. 3). Thus the high level of noise in phase-coupling FC might be a factor in the difference of EEG and fMRI connectivity.

Interestingly, previous work has identified some overlap between EEG and fMRI FC (Wirsich et al., 2017). On the other hand, EEG FC was complementary to fMRI FC in predicting anatomical connectivity (Wirsich et al., 2017). This suggests that part of the EEG FC is distinct from fMRI FC. This observation has also been confirmed by a study analysing phase-coupling ICA networks (Wirsich et al., 2020). It is plausible that phase coupling FC captures networks that are distinct from fMRI, while amplitude coupling FC capture similar networks (Brookes et al., 2011a, 2011b; Hiltunen et al., 2014; Hipp and Siegel, 2015; Liu et al., 2018, 2017; Pasquale et al., 2010). Amplitude and phase couling measures are both influenced by the phase and therefore it is hard to compare previous results using each measure (Palva et al., 2018). A recent study that investigated the direct relationship of phase- and amplitude-coupling measures in MEG further discusses this issue (Siems and Siegel, 2020). Despite their differences, some similarities in the network structure are found between phase- and amplitude-coupling measures (Demuru et al., 2020).

3.4. Relationship to previous literature on associations of FC with phenotype in fMRI

Several studies have investigated the spatial patterns of differences of fMRI FC driven by various phenotypes (Biswal et al., 2010; Finn et al., 2015; Shehzad et al., 2014; Simard et al., 2015; Smith et al., 2015). Upon visual inspection the spatial patterns of connectivity-phenotype relationships found in these publications overlap in some of the parcels we have

identified but overall are different. A notable exception are the results in Smith et al. (2015), which indicates a strong relationship of the default mode network to a combination of "positive" phenotypes that resembles the pattern of fMRI connectivity-IQ relationship we report in Fig. 8. While the "positive" phenotypes in Smith et al. (2015), are largely driven by fluid intelligence they include other measures for language, working memory and attention. This confounds the comparison to our results.

3.5. Reliability of FC in fMRI and EEG

Reliability of fMRI FC increases from 2.5 to 5 min of recording time for both resting state and video data (Fig. 3C and D) consistent with O'Connor et al. (O'Connor et al., 2017). Spatial patterns of reliability of FC (Fig. A3) are roughly similar to those previously reported (O'Connor et al., 2017). Specifically, high reliability in the visual network has been reported (Schmäalzle et al., 2017). An exception is that reliability in the visual network does not differ much in our data between the resting state and video task (Fig. A3). Such a difference between resting state and video conditions has been observed in O'Connor et al. (O'Connor et al., 2017). This might stem from differences in subjects keeping their eyes open or closed (Patriat et al., 2013).

Lacking suitable data to measure the reliability of EEG FC with recording time (Fig. 1C) we investigate the difference in reliability across tasks for different frequency bands. We have found that the reliability of FC increases with frequency (Fig. 3B). This may be the result of more focal activity as frequency increases (Freeman et al., 2003, 2000) and thus inverse modeling is more reliable. We conclude that EEG connectivity phenotype relationships are most reliably measured in the high frequency bands, especially the beta band.

3.6. Caveats and alternative approaches

The imaginary part of coherency is robust to artifacts of volume conduction (Nolte et al., 2004; Palva et al., 2018). Some issues with this measure remain: True interactions with a close to zero-phase time lag are excluded, the strength of connectivity depends on the phase, and spurious correlations are still present (Palva et al., 2018). New methods have been proposed to alleviate these spurious "ghost interactions" for amplitude coupling (Wang et al., 2018). Future studies have to develop similar methods for phase couling measures.

The total length of recordings included in this study is about 23 min (Fig. 1C) and at the lower end of the recommended 25 min to measure reliable connectivity in fMRI (Elliott et al., 2019; Laumann et al., 2015). Using additional task paradigms, which are available for EEG in this dataset (Alexander et al., 2017), could improve reliability of EEG connectivity. However, we intentionally constrained ourselves to "passive" tasks so as to be comparable to previous FC work on fMRI.

We have used Pearson's correlation to quantify the similarity of connectivity patterns. Other measures, such as Euclidean distance, can also capture differences of means and have been discussed in Shehzad et al. (2014). In fact, the absolute median difference between male and female subjects in each channel pair is most distinct within the visual cortex (Fig. A.9). On the contrary, we find the strongest connectivity-sex relationship with MDMR for connections between the visual and the attention, frontoparietal and default mode networks

(Fig. 6). The absolute median difference is driven by absolute differences in strength of connectivity at each link, while MDMR compares the similarity of patterns of connectivity within and between networks. Alternative analysis methods such as Joint and Individual Variation Explained (JIVE) (Lock et al., 2013; Yu et al., 2017) or Multiscale Graph Correlation (Shen et al., 2018; Vogelstein et al., 2019) give us similar results for MDMR (Fig. A7).

We have chosen a functional cortical parcellation for practical purposes. The Schaefer atlas is available in volume and surface space. Different cortical parcellations could change the subject-by-subject similarity and in consequence the connectivity-phenotype relationship. However, using an anatomical parcellation (Desikan et al., 2006) we find very similar connectivity-phenotype relationships (Fig. A.11). Similarly, we expect that using a clustering of connectivity as proposed by Wang et al. would not influence the connectivity-phenotype relationships (Wang et al., 2018). Conversely, it has been suggested to use parcellations defined on EEG or MEG to improve signal-to-noise ratio (Colclough et al., 2016). Indeed, we have shown that clustering of EEG and fMRI connectivity is distinct (Fig. 2). A note of caution on the clustering of EEG functional connectivity is that the spatially contiguous parcels of connectivity might be enhanced by “ghost interactions” (Palva et al., 2018; Wang et al., 2018). These spurious correlations in the vicinity of true interactions can result from local field spread or genuine short-range connectivity.

Our subjects population consists of both healthy subjects and those exhibiting developmental psychopathology (Alexander et al., 2017). It is known that several of the phenotypes investigated in this study are correlated to each other. Socioeconomic status, for example, has a strong influence on IQ (Hanscombe et al., 2012; Turkheimer et al., 2003). Similarly, it has been shown that subjects with autism rely more on connectivity in visual areas when solving tasks in IQ tests than healthy subjects (Simard et al., 2015). Only ~12% of subjects in our sample have been diagnosed with autism; therefore interactions with IQ are unlikely in our data. However, the interactions between different psychiatric phenotypes should be the subject of future studies.

We have identified a number of possible anatomical confounds, that differ with age and sex such as head size (Fig. A4) or cardiac artifacts (Fig. A5A). The effect of this would be expected to be broadly distributed (in contrast to findings in Figs. 6 and 7) and should have the same sign in different frequency bands (in contrast to findings in Fig. A.9). Age and sex effects could also influence the analysis of within- and between-subject correlation of FC (Fig. 3). Specifically, the lower between-subject correlation could results from anatomical differences in age and sex. However, this has been explicitly controlled for in the fMRI data and we do not expect that age and sex differences account for all the differences of connectivity between different subjects. Thus, while we do not rule out such confounds, we suggest that purely neurological factors may play a role in the age and sex effects. Future studies will be necessary to clearly dissociate anatomical and neurological effects of age, sex, head size and cardiac artifacs on FC in EEG.

3.7. Future directions

Given the different physiological origin of EEG and fMRI as well as differences in connectivity measures (Haufe et al., 2018; Siems and Siegel, 2020; Wirsich et al., 2020), it is not surprising that we do not find any similarities between the connectivity matrices. However, it has been shown that the two measures capture complementary information of connectivity (Wirsich et al., 2017). In light of this, making use of simultaneous EEG and fMRI recordings opens new possibilities in investigating the properties and behavioral relevance of FC. Investigating the differences of FC patterns in different modalities can improve the understanding of the physiological origin of FC. Further, by combining data from EEG and fMRI, subject identification by FC and the connectivity-phenotype relationship could be improved. In contrast to fMRI, EEG FC allows the analysis of FC on a faster timescale and a more detailed analysis of directed FC. This can be useful in the context of the recent effort to extend FC analysis by a causality framework (Reid et al., 2019).

4. Conclusion

We have systematically investigated the FC measured with phase-coupling of EEG and compare this to phenotypic and demographic variables as well as to FC in fMRI. Using a large database we were able to show that EEG FC networks are similar in robustness to fMRI networks. Specifically, EEG FC networks are most robust in the higher frequency bands, such as the beta band. As reported in the fMRI literature, functional networks are more similar between tasks measured in the same subject than between different subjects during the same task. The relationship between whole-brain EEG FC and various phenotypes is similar to that observed for fMRI. Therefore, EEG has the potential to predict behavior comparable to fMRI. We have shown that the functional organization of the cortex look different when measured with phase-coupling of EEG than fMRI. We hope that this work provides the basis for a new research direction in FC based on EEG, that is distinct from the functional network established with fMRI.

5. Methods

5.1. Participants and tasks

Participants recruited through the HBN initiative are children and adolescents aged 5–21. A diverse sample has been collected from the New York City area including a large proportion of subjects with psychiatric disorders (Alexander et al., 2017). We analyzed both fMRI scans and EEG recordings available on the HBN Biobank. For fMRI we used FC data of participants during resting state (two sessions of 300 s each) and watching naturalistic stimuli (‘The Present’; duration 201 s, and ‘Despicable Me’, duration 600 s). This dataset consists of fMRI scans from 766 participants. We included EEG data from the first six releases, with a total of 1657 subjects. Depending on availability and data quality we combined several paradigms; resting state (duration 300 s), two blocks of the inhibition/excitation paradigm (duration 210 s each), and four naturalistic stimuli (‘Despicable Me’, duration 170 s, ‘The Present’, duration 230 s, ‘Diary of a Wimpy Kid’, duration 117 s, and ‘Fun with Fractals’, duration 163 s) (Fig. 1C).

Data collection for the Healthy Brain Networks Biobank is described in detail elsewhere (Alexander et al., 2017). Briefly, EEG is recorded using a 128-channel EEG geodesic hydrocel system by Electrical Geodesics Inc. (EGI) with a reference at the vertex of the head (Cz). fMRI data is recorded at different sites with varying scanner parameters.

5.2. Phenotypic data

The HBN dataset includes several psychiatric, behavioral, cognitive, and lifestyle phenotypes collected with standard assessment instruments (Alexander et al., 2017). All analysis has been conducted in MATLAB R2019b (Natick, MA, The MathWorks Inc.) A data driven approach was applied to select a subset of these phenotypes for further analysis. First, the total scores of all available assessments were retrieved from the database, subscores were not included. Phenotypes that capture exclusively physical features were excluded (e.g fitness level, bio-electric impedance analysis, pregnancy). Of the remaining 47 phenotypes, ten were selected in two steps. First, 22 phenotypes with more than 50% missing data were excluded. Data of the remaining phenotypes was normalized by z-scoring. Missing values in the remaining data were estimated using the alternating least squares (ALS) algorithm (Ilin and Raiko, 2010; Roweis, 1998). Principal component analysis (PCA) was applied on the data including the estimate of missing values. The PCA coefficients of the components explaining at least 40% of the variance (3 top components) were averaged and the phenotypes with the largest average coefficients were selected for further analysis.

5.3. EEG preprocessing

We developed an algorithm for automated preprocessing of EEG data to handle the large amount of data in the HBN database. Since FC measures the consistency of phase between channels, special care was taken to use filters that do not distort phase. Subspace projection methods such as PCA and ICA might introduce dependencies between channels and were not applied to the data. The preprocessing algorithm consists of a number of steps removing artifactual samples and channels based on statistical thresholds. 1) Zero phase 5th order Butterworth filters are applied to remove drift (0.5 Hz high-pass) and line noise (60 Hz and harmonics). 2) Channels without signal or with large portions of flat signal (>5 s) are removed. 3) Channels whose standard deviation is larger than 2 times the interquartile range of the standard deviations across all channels are rejected. 4) The effect of eyeblinks and eye movements are removed from the EEG data by subtracting the signal estimated by a least squares regression model using EOG channels (Repov s, Grega, 2010). 5) Channels of high frequency power are removed by computing the ratio of the standard deviation of the high-passed signal (35 Hz cutoff) over the standard deviation of the signal with full frequency spectrum. Similar to step 3) a channel is excluded when the ratio of the standard deviation of high frequency versus the full spectrum is above 2 times the interquartile range across channels. 6) Samples with an absolute voltage above 4 times the interquartile range of voltage per channel are removed. 7) To remove high-frequency samples the data is high-pass filtered (5th order zero-phase Butterworth filter with a cutoff at 35 Hz) and split into segments of 200 ms. Epochs are z-scored across channels and time points and epochs with a z-score above 4 are rejected (Mahjoory et al., 2017). For steps 8–10) steps 3, 8 and 9 are repeated. With overall cleaner data more artifacts can be removed through a second pass. 11) Channels that have more than 25% of data removed though the previous steps are removed

completely. 12) Removed samples are interpolated from other channels if at least two thirds of the samples at the same time point are available in other channels (Madsen et al., 2019). Other samples are set to zero and the edges are smoothed by a mask. 13) The cardiac artifact occurs in similar channels in different subjects. Peaks of the cardiac artifact do not occur at a precise frequency and their amplitude is often similar to the neural signal. We use a subspace subtraction method to remove the artifact, similar to what is used for electro-ballistogram removal in fMRI. Specifically, we visually inspect the EEG to identify channels with obvious cardiac signals (Fig. A5A). A peak-finding routine is applied and the signal in a window of 264 ms (33 samples at 125 Hz) surrounding each peak is selected. Principal components analysis of this data identifies the subspace that dominates the artifact and this subspace is subtracted from the EEG (Parra et al., 2005). This procedure is only applied if an electrode is found with an obvious cardiac signal.

5.4. Movement artifacts

FC in channels on the neck are most strongly affected by differences in sex (data not shown). This effect is most likely due to movement artifacts. Channels close to neck and face have been excluded from the analysis to reduce the effects of movement artifacts that have not been removed by the preprocessing algorithm. 38 channels with the following labels in the 128 channel EGI Geodesic Sensor Net were excluded: E1, E8, E14, E17, E21, E25, E32, E38, E43, E44, E48, E49, E56, E57, E63, E64, E69, E73, E74, E81, E82, E88, E89, E94, E95, E99, E100, E107, E113, E114, E119, E120, E121, E125, E126, E127, E128.

5.5. Automated rating of data quality

Data quality is rated by four criteria: 1) The number of bad channels removed by the preprocessing algorithm. 2) The number of samples rejected as artifacts divided by the total number of samples. 3) The ratio of samples with an absolute voltage above 15 mV. 4) Time points with a standard deviation across channels above 14 mV. Only time points that include at least 30% of samples across channels are included in measuring standard deviation.

For each measure a rating from 1 (worst) to 5 (best) is assigned based on the distribution of quality measures over all subjects. The percentile thresholds are given in Table 1. The total rating per subject is the mean of the ratings assigned to all four measures. If the rating of high voltage or high variance is only 1 or 2 the overall rating is set to 1. This ensures that subjects with very bad quality in one measure are excluded from the analysis. Recordings with low sum of power across channels ($<3*10^5$ mV^2) are also set to a rating of 1. Ratings 4 and 5 describe data of reasonably good quality which was included in the analysis. In total 1330 subjects have at least one recording with a rating of 4 or 5 (Fig. 1).

5.6. Source reconstruction

Source reconstruction was conducted for every subject based on the (Fischl et al., 1999). The leadfield was created with Brainstorm (Tadel et al., 2011) and OpenMEEG (Gramfort et al., 2010; Kybic et al., 2005) using a 3-shell BEM model and the EGI Hydrocel 129 cap. We imported the 200 parcel parcellation matched to the Yeo 7 network parcellation defined by Schaefer et al. (2018). The pial surface of the fsaverage standard head was resampled to 2003 voxels using Matlab's reducepatch method. The BEM model consists of a scalp layer

with 1082 voxels and a relative conductivity of 1, a skull layer with 1922 voxels and a relative conductivity of 0.0125 and a brain layer with 1922 voxels and a relative conductivity of 1. The OpenMEEG head model was computed using adaptive integration. Before source reconstruction, both the EEG data and the head model were converted to a common average reference. This has been done, because it is important that forward model and electrode reference match one another (Nunez and Srinivasan, 2016; Pascual--Marqui et al., 2011). EEG data is projected into source space by the eLORETA inverse projection kernel with 5% regularization (Pascual--Marqui, 2007). Signals in source space are then z-scored. For each region of interest in the Schaefer atlas the strongest 3 PCA components of the source space signal are selected. iCOH is calculated in source space for each PCA component separately. To account for the random polarity of the source signals introduced by the source reconstruction and PCA steps, the absolute value was taken. The final FC matrix consists of the mean connectivity across the three PCA components per region of interest. Computing connectivity on PCA components mitigates the effect of signals leaking from a parcellation to others.

5.7. fMRI preprocessing

The fMRI data were preprocessed using the Configurable Pipeline for the Analysis of Connectomes (C-PAC) (Craddock et al., 2013). The structural preprocessing includes: 1) Brain extraction using AFNI, 2) tissue segmentation using FAST, 3) registration to the MNI152 template using ANTs. The functional preprocessing includes: 1) Motion correction, 2) motion spiking regression with mean framewise displacement threshold at 0.5 mm, 3) nuisance regression with aCompCor, cerebro-spinal fluid, and Friston-24 motion parameters, 4) linear and quadratic detrending, 5) band-pass filtering (0.01–0.1 Hz), 6) boundary-based co-registration from functional space to native anatomical space and subsequent registration to MNI152 template space, 7) projection from MNI152 vol space to the Freesurfer subject surface space and down-sampling to a 10k resolution surface (10,242 voxels per hemisphere).

5.8. Functional connectivity

A common measure for FC is coherency, a measure of phase synchronicity between two signals (Bastos and Schoffelen, 2016; Mahjoory et al., 2017). Coherency is a complex-valued quantity reflecting the average phase difference between two time series as well as the stability of that difference across repeated measurements. In many application domains, the absolute value of coherency (referred to as coherence) is used to obtain a metric of phase coupling that is independent of the actual delay between the time series. In EEG, however, it is necessary to distinguish zero from non-zero phase delays as zero-lag interactions are likely to have trivial origin. Since EEG electrodes measure a mixture of signals from several neural sources through instantaneous volume conduction from the brain to the scalp, electrodes appear to be coherent with zero delay as the signal from one neural source arrives at several electrodes at the same time. The same holds true for reconstructed source activity, for which the instantaneous mixing introduced by volume conduction can in general not be undone completely. To prevent spurious connectivity due to source mixing the imaginary part of coherency (iCOH) can be employed (Nolte et al., 2004). iCOH is robust to volume conduction artifacts in function connectivity by excluding coherency at zero phase delay.

The FC matrices are calculated in MATLAB using the FieldTrip Toolbox (Oostenveld et al., 2011) based on an implementation described previously (Bastos and Schoffelen, 2016; Nolte et al., 2004). First, the Fourier spectrum of the preprocessed EEG signal is computed using multi taper frequency transformation with discrete prolate spheroidal sequences. The cross-spectral density is then computed from the Fourier spectrum by multiplying the Fourier spectrum of the signal of one EEG channel with the complex conjugate of the Fourier spectrum of all other channels and averaging over epochs of 2 s. Epochs are averaged over trials of all EEG source space data of all tasks with good data quality, as defined above. iCOH is the absolute value of the imaginary part of the cross-spectral density scaled by the square root of the product of the power of the signal of each channel. By creating epochs of 2s an iCOH matrix can be calculated for frequencies of 0.5 Hz and above. iCOH matrices were computed for 126 frequency between 0.5 Hz and 62.5 Hz with a resolution of 0.5 Hz. To obtain an iCOH matrix for each frequency band, iCOH values for each pair of parcellations were averaged across all bins within a band. The delta band is defined between 0.5 and 4 Hz, the theta band between 4 and 7.5 Hz, the alpha band between 7.5 and 15 Hz and the beta band between 15 and 30 Hz.

FC in fMRI is measured by Pearson's correlation between the time series of activations between each pair of parcellations in the Schaefer atlas.

5.9. Clustering of EEG FC

The clusters for the EEG FC shown in Fig. 2A were computed using the method described in Yeo et al. (2011) (Yeo et al., 2011). All EEG source space FC matrices are computed for each frequency band as defined above. The average of the connectivity matrices using all 2003 voxels on the cortical surface mesh is computed across all subjects with good data quality. Then the connectivity is averaged in 200 parcels of the Schaefer atlas (Schaefer et al., 2018) to reduce the feature dimensions by a factor roughly 10. This creates 2003 voxels in 200 feature dimensions. These voxels are then grouped into 7 clusters separately per hemisphere by minimizing the geodesic distance between the voxels in each cluster on a 200 dimensional hypersphere (Lashkari et al., 2010; Yeo et al., 2011). The clusters are reordered and colored in Fig. 2A so that the clusters that are located in similar structures for each hemisphere and band are colored the same. The confusion matrices in Fig. 2B are computed by counting the number of voxels in the same or different clusters, respectively. The number of voxels assigned to the same clusters in two conditions are plotted on the diagonal, voxels assigned to different clusters are plotted on the off-diagonal. Precision is measured by the ratio of voxels assigned to the same clusters over the total number of voxels. A precision of 1 would indicate that every vertex is assigned to the same cluster in both conditions, 0 that all voxels are assigned to different clusters.

5.10. Comparing EEG and fMRI connectivity matrices

Four methods have been used to assess the similarity of EEG and fMRI connectivity matrices, Pearson's correlation, the image intraclass correlation coefficient (I2C2) (Shou et al., 2013), Multiscale Graph Correlation (MGC) algorithm (Shen et al., 2018; Vogelstein et al., 2019) and geodesic distance (Venkatesh et al., 2020). To establish statistical significance of these distance measures we shuffle the subjects labels and compute the distance measures

between the new pairs (Lai et al., 2018; Venkatesh et al., 2020). 1000 permutations were performed for each measure and frequency band. In the case of I2C2 we perform bootstrapping as discussed in Shou et al. (2013).

5.11. Multivariate distance matrix regression (MDMR)

To compare whole-brain FC to phenotypes first a subject-by-subject distance matrix of whole brain FC is calculated. To this end, the iCOH connectivity matrix between areas of the Shaefer atlas was arranged as a vector by stacking its columns. Subjects with short recordings below 20s were excluded. The vectorized connectivity matrices were then concatenated into a m-by-n matrix, where m is the number of subjects and n is the square of the number of areas in the Schaefer parcellation. The m-bym subject-by-subject distance matrix is obtained by calculating Pearson's correlation coefficient for each pair of rows of this matrix.

We repeat this analysis resolved in space, namely, instead of the whole-brain FC we now analyze the connectivity emanating from a single parcellation area. Thus the m-by-n matrix now refers to m subjects and n parcellation areas. Lastly, distance matrices relating to networks defined by Yeo et al. are computed by selecting the submatrices containing parcellations corresponding to each network.

MDMR tests whether subjects with similar connectivity also have similar phenotypes (Shehzad et al., 2014). The pseudo F-statistic is a measure of the ratio of hypothesis-sums-of-squares to residual-sums-of-squares following a linear model relating the subject-by-subject distance matrix to the phenotypic data (Mcardle and Anderson, 2001). Since the distribution of the pseudo F-statistic is unknown, significance is assessed by establishing an empirical null distribution. This is achieved by recomputing the pseudo F-Statistic after shuffling the subject labels of the distance matrix (Shehzad et al., 2014).

Not every subject includes a full set of phenotypic measures. MDMR is computed on the subset of FC matrices with matching phenotypes data separately for each phenotype.

Several of the selected phenotypes are strongly correlated to sex, age or head size. ADHD, for example, is diagnosed more often in boys than girls. MDMR can be formulated to test the association of a subject-by-subject distance matrix to phenotypes taking into account nuisance covariates (Reiss et al., 2010; Shehzad et al., 2014). The effects of age, sex and head size can be arranged in a design matrix that is subtracted from the design matrix including the phenotype of interest. The Pseudo F-statistic then measures the connectivity-phenotype relationship controlled for nuisance covariates.

To account for multiple comparisons the Benjamini-Hochberg procedure to correct for false discoveries is applied (Benjamini and Hochberg, 1995). The procedure limits the false discovery rate (FDR; rate of type-I errors) to $\alpha = 0{:}05$. MATLAB's implementation of the Benjamini-Hochberg procedure is used.

5.12. Visualization

The value of the pseudo F-statistic describing the strength of the connectivity-phenotype association in a cortical parcellation is plotted on a smoothed fsaverage surface (Haufe and Ewald, 2019). Sources on the medial surface are not meaningful in the EEG analysis and are not shown but included in the analysis.

5.13. Reliability of measurements

Reliability of connectivity measurements was tested for each possible pair of connectivity between parcellations. The measure used was intraclass-correlation (ICC). ICC was measured between actual or virtual sessions in the case of fMRI and between tasks (resting state, excitation/inhibition paradigm and videos) in EEG. For this purpose the ICC(3,1) model was chosen to measure consistency between sessions or tasks (McGraw and Wong, 1996). ICC(3,1) is based on a mixed effect model. The measure of FC is modeled by a fixed effect of sessions or task, and a random effect of subjects. ICC(3,1) is defined as the variance between subjects divided by the total variance. The total variance is the sum of the variance between subjects and the variance between tasks. An ICC(3,1) value of 1 would indicate perfect consistency between sessions or tasks. An ICC(3,1) value of 0 would indicate that subjects have the same values.

fMRI data for each 5 min resting state session was split into two virtual sessions of 2.5 min each. FC matrices were computed for each virtual session. ICC(3,1) between all possible combinations of 2.5 min virtual sessions was computed and averaged. Further, ICC(3,1) was computed between the actual 5 min resting state sessions. For the video task we compare connectivity matrices computed for virtual sessions of 2.5 and 5 min generated from the same recording session. Statistical significance of the difference between ICC(3,1) for 2.5 min and 5 min was tested with a Wilcoxon signed rank test across all pairs of connectivity. The analysis was conducted using data from 359 subjects for which data were available for each condition.

For the EEG analysis iCOH matrices were computed for each task (resting state, excitation/inhibition paradigm and videos) after concatenating all available sessions within each task. ICC(3,1) was computed for all pairs of parcellations separately for each frequency band. Amongst all subjects with data available for all sessions in all tasks, 50 subjects with the best data quality were selected for this analysis.

Supplementary Material

Refer to Web version on PubMed Central for supplementary material.

Acknowledgements

This research was supported by a National Institute of Health (NIH) grant 1R01MH111439 and by the European Research Council (ERC) under the European Union’s Horizon 2020 research and innovation programme (Grant agreement No. 758985).

We thank Lindsay Alexander, MPH for her help on interpreting the phenotypic data.

References

Alexander LM, Escalera J, Ai L, Andreotti C, Febre K, Mangone A, Vega-Potler N, Langer N, Alexander A, Kovacs M, Litke S, O'Hagan B, Andersen J, Bronstein B, Bui A, Bushey M, Butler H, Castagna V, Camacho N, Chan E, Citera D, Clucas J, Cohen S, Dufek S, Eaves M, Fradera B, Gardner J, Grant-Villegas N, Green G, Gregory C, Hart E, Harris S, Horton M, Kahn D, Kabotyanski K, Karmel B, Kelly SP, Kleinman K, Koo B, Kramer E, Lennon E, Lord C, Mantello G, Margolis A, Merikangas KR, Milham J, Minniti G, Neuhaus R, Levine A, Osman Y, Parra LC, Pugh KR, Racanello A, Restrepo A, Saltzman T, Septimus B, Tobe R, Waltz R, Williams A, Yeo A, Castellanos FX, Klein A, Paus T, Leventhal BL, Craddock RC, Koplewicz HS, Milham MP, 2017 An open resource for transdiagnostic research in pediatric mental health and learning disorders. Sci. Data 4, 170181 10.1038/sdata.2017.181. [PubMed: 29257126]

Anzolin A, Presti P, Van De Steen F, Astolfi L, Haufe S, Marinazzo D, 2019 Quantifying the effect of demixing approaches on directed connectivity estimated between reconstructed EEG sources. Brain Topogr 32, 655–674. 10.1007/s10548-019-00705-z. [PubMed: 30972604]

Bastos AM, Schoffelen J-M, 2016 A tutorial review of functional connectivity analysis methods and their interpretational pitfalls. Front. Syst. Neurosci 9 10.3389/fnsys.2015.00175.

Bathelt J, O'Reilly H, Clayden JD, Cross JH, de Haan M, 2013 Functional brain network organisation of children between 2 and 5 years derived from reconstructed activity of cortical sources of high-density EEG recordings. Neuroimage 82, 595–604. 10.1016/j.neuroimage.2013.06.003. [PubMed: 23769920]

Benjamini Y, Hochberg Y, 1995 Controlling the false discovery rate: a practical and powerful approach to multiple testing. J. R. Stat. Soc. Ser. B Methodol 57, 289–300. 10.1111/j.2517-6161.1995.tb02031.x.

Biswal B, Zerrin Yetkin F, Haughton VM, Hyde JS, 1995 Functional connectivity in the motor cortex of resting human brain using echo-planar mri. Magn. Reson. Med 34, 537–541. 10.1002/mrm.1910340409. [PubMed: 8524021]

Biswal BB, Mennes M, Zuo X-N, Gohel S, Kelly C, Smith SM, Beckmann CF, Adelstein JS, Buckner RL, Colcombe S, Dogonowski A-M, Ernst M, Fair D, Hampson M, Hoptman MJ, Hyde JS, Kiviniemi VJ, Kötter R, Li S-J, Lin C-P, Lowe MJ, Mackay C, Madden DJ, Madsen KH, Margulies DS, Mayberg HS, McMahon K, Monk CS, Mostofsky SH, Nagel BJ, Pekar JJ, Peltier SJ, Petersen SE, Riedl V, Rombouts SARB, Rypma B, Schlaggar BL, Schmidt S, Seidler RD, Siegle GJ, Sorg C, Teng G-J, Veijola J, Villringer A, Walter M, Wang L, Weng X-C, Whitfield-Gabrieli S, Williamson P, Windischberger C, Zang Y-F, Zhang H-Y, Castellanos FX, Milham MP, 2010 Toward discovery science of human brain function. Proc. Natl. Acad. Sci 107, 4734–4739. 10.1073/pnas.0911855107. [PubMed: 20176931]

Brookes MJ, Hale JR, Zumer JM, Stevenson CM, Francis ST, Barnes GR, Owen JP, Morris PG, Nagarajan SS, 2011a Measuring functional connectivity using MEG: Methodology and comparison with fcMRI. Neuroimage 56, 1082–1104. 10.1016/j.neuroimage.2011.02.054. [PubMed: 21352925]

Brookes MJ, Tewarie PK, Hunt BAE, Robson SE, Gascoyne LE, Liddle EB, Liddle PF, Morris PG, 2016 A multi-layer network approach to MEG connectivity analysis. Neuroimage 132, 425–438. 10.1016/j.neuroimage.2016.02.045. [PubMed: 26908313]

Brookes MJ, Woolrich M, Luckhoo H, Price D, Hale JR, Stephenson MC, Barnes GR, Smith SM, Morris PG, 2011b Investigating the electrophysiological basis of resting state networks using magnetoencephalography. Proc. Natl. Acad. Sci 108, 16783–16788. 10.1073/pnas.1112685108. [PubMed: 21930901]

Bullmore E, Fadili J, Maxim V, Şendur L, Whitcher B, Suckling J, Brammer M, Breakspear M, 2004 Wavelets and functional magnetic resonance imaging of the human brain. NeuroImage 23 (Supplement 1), S234–S249. 10.1016/j.neuroimage.2004.07.012. [PubMed: 15501094]

Bullmore E, Sporns O, 2009 Complex brain networks: graph theoretical analysis of structural and functional systems. Nat. Rev. Neurosci 10, 186–198. 10.1038/nrn2575. [PubMed: 19190637]

Bullmore ET, Bassett DS, 2011 Brain graphs: graphical models of the human brain connectome. Annu. Rev. Clin. Psychol 7, 113–140. 10.1146/annurev-clinpsy-040510-143934. [PubMed: 21128784]

Colclough GL, Woolrich MW, Tewarie PK, Brookes MJ, Quinn AJ, Smith SM, 2016 How reliable are MEG resting-state connectivity metrics? Neuroimage 138, 284–293. 10.1016/j.neuroimage.2016.05.070. [PubMed: 27262239]

Cole MW, Bassett DS, Power JD, Braver TS, Petersen SE, 2014 Intrinsic and task-evoked network architectures of the human brain. Neuron 83, 238–251. 10.1016/j.neuron.2014.05.014. [PubMed: 24991964]

Conner CR, Ellmore TM, Pieters TA, DiSano MA, Tandon N, 2011 Variability of the relationship between electrophysiology and BOLD-fMRI across cortical regions in humans. J. Neurosci 31, 12855–12865. 10.1523/JNEUROSCI.1457-11.2011. [PubMed: 21900564]

Coquelet N, Mary A, Peigneux P, Goldman S, Wens V, Tiége XD, 2017 The electrophysiological connectome is maintained in healthy elders: a power envelope correlation MEG study. Sci. Rep 7, 1–10. 10.1038/s41598-017-13829-8. [PubMed: 28127051]

Craddock C, Sikka S, Cheung B, Khanuja R, Ghosh SS, Yan C, Li Q, Lurie D, Vogelstein J, Burns R, Colcombe S, Mennes M, Kelly C, Di Martino A, Castellanos FX, Milham M, 2013 Towards automated analysis of connectomes: the configurable pipeline for the analysis of connectomes (C-PAC). In: Presented at the Front. Neuroinform. Conference Abstract 10.3389/conf.fninf.2013.09.00042. Stockholm, Sweden.

Dadi K, Rahim M, Abraham A, Chyzhyk D, Milham M, Thirion B, Varoquaux G, 2019 Benchmarking functional connectome-based predictive models for resting-state fMRI. Neuroimage 192, 115–134. 10.1016/j.neuroimage.2019.02.062. [PubMed: 30836146]

Demuru M, La Cava SM, Pani SM, Fraschini M, 2020 A comparison between power spectral density and network metrics: an EEG study. Biomed. Signal Process Contr 57, 101760 10.1016/j.bspc.2019.101760.

Desikan RS, S egonne F, Fischl B, Quinn BT, Dickerson BC, Blacker D, Buckner RL, Dale AM, Maguire RP, Hyman BT, Albert MS, Killiany RJ, 2006 An automated labeling system for subdividing the human cerebral cortex on MRI scans into gyral based regions of interest. Neuroimage 31, 968–980. 10.1016/j.neuroimage.2006.01.021. [PubMed: 16530430]

Elliott ML, Knodt AR, Cooke M, Kim MJ, Melzer TR, Keenan R, Ireland D, Ramrakha S, Poulton R, Caspi A, Moffitt TE, Hariri AR, 2019 General functional connectivity: shared features of resting-state and task fMRI drive reliable and heritable individual differences in functional brain networks. Neuroimage 189, 516–532. 10.1016/j.neuroimage.2019.01.068. [PubMed: 30708106]

Ezaki T, Reis E.F.dos, Watanabe T, Sakaki M, Masuda N, 2019 Critical Brain Dynamics and Human Intelligence 10.1101/688655 bioRxiv 688655.

Finn ES, Shen X, Scheinost D, Rosenberg MD, Huang J, Chun MM, Papademetris X, Constable RT, 2015 Functional connectome fingerprinting: identifying individuals using patterns of brain connectivity. Nat. Neurosci 18, 1664–1671. 10.1038/nn.4135. [PubMed: 26457551]

Fischl B, Sereno MI, Tootell RBH, Dale AM, 1999 High-resolution intersubject averaging and a coordinate system for the cortical surface. Hum. Brain Mapp 8, 272–284. 10.1002/(SICI)1097-0193(1999)8:4<272::AIDHBM10>3.0.CO;2-4. [PubMed: 10619420]

Fornito A, Zalesky A, Pantelis C, Bullmore ET, 2012 Schizophrenia, neuroimaging and connectomics. NeuroImage 62, 2296–2314. 10.1016/j.neuroimage.2011.12.090. Connectivity. [PubMed: 22387165]

Fox MD, Raichle ME, 2007 Spontaneous fluctuations in brain activity observed with functional magnetic resonance imaging. Nat. Rev. Neurosci 8, 700–711. 10.1038/nrn2201. [PubMed: 17704812]

Freeman WJ, Holmes MD, Burke BC, Vanhatalo S, 2003 Spatial spectra of scalp EEG and EMG from awake humans. Clin. Neurophysiol 114, 1053–1068. 10.1016/S1388-2457(03)00045-2. [PubMed: 12804674]

Freeman WJ, Rogers LJ, Holmes MD, Silbergeld DL, 2000 Spatial spectral analysis of human electrocorticograms including the alpha and gamma bands. J. Neurosci. Methods 95, 111–121. 10.1016/S0165-0270(99)00160-0. [PubMed: 10752481]

Fries P, 2005 A mechanism for cognitive dynamics: neuronal communication through neuronal coherence. Trends Cognit. Sci 9, 474–480. 10.1016/j.tics.2005.08.011. [PubMed: 16150631]

Fujimoto T, Okumura E, Kodabashi A, Takeuchi K, Otsubo T, Nakamura K, Yatsushiro K, Sekine M, Kamiya S, Shimooki S, Tamura T, 2016 Sex differences in gamma band functional connectivity between the frontal lobe and cortical areas during an auditory oddball task, as revealed by imaginary coherence assessment. Open Neuroimaging J 10, 85–101. 10.2174/1874440001610010085.

Gao S, Greene AS, Constable RT, Scheinost D, 2019 Combining multiple connectomes improves predictive modeling of phenotypic measures. Neuroimage 201, 116038 10.1016/j.neuroimage.2019.116038. [PubMed: 31336188]

Geerligs Linda, Renken RJ, Saliasi E, Maurits NM, Lorist MM, 2015a A brain-wide study of age-related changes in functional connectivity. Cerebr. Cortex 25, 1987–1999. 10.1093/cercor/bhu012.

Geerligs L, Rubinov M, Cam-Can, Henson RN, 2015b State and trait components of functional connectivity: individual differences vary with mental state. J. Neurosci 35, 13949–13961. 10.1523/JNEUROSCI.1324-15.2015. [PubMed: 26468196]

Gramfort A, Papadopoulo T, Olivi E, Clerc M, 2010 OpenMEEG: opensource software for quasistatic bioelectromagnetics. Biomed. Eng. Online 9, 45 10.1186/1475-925X-9-45. [PubMed: 20819204]

Hacker CD, Snyder AZ, Pahwa M, Corbetta M, Leuthardt EC, 2017 Frequency-specific electrophysiologic correlates of resting state fMRI networks. Neuroimage 149, 446–457. 10.1016/j.neuroimage.2017.01.054. [PubMed: 28159686]

Hall EL, Robson SE, Morris PG, Brookes MJ, 2014 The relationship between MEG and fMRI. NeuroImage 102, 80–91. 10.1016/j.neuroimage.2013.11.005. Multimodal Data Fusion. [PubMed: 24239589]

Hanscombe KB, Trzaskowski M, Haworth CMA, Davis OSP, Dale PS, Plomin R, 2012 Socioeconomic status (SES) and children's intelligence (IQ): in a UK-representative sample SES moderates the environmental, not genetic, effect on IQ. PloS One 7, e30320 10.1371/journal.pone.0030320. [PubMed: 22312423]

Haufe S, DeGuzman P, Henin S, Arcaro M, Honey CJ, Hasson U, Parra LC, 2018 Elucidating relations between fMRI, ECoG, and EEG through a common natural stimulus. Neuroimage 179, 79–91. 10.1016/j.neuroimage.2018.06.016. [PubMed: 29902585]

Haufe S, Ewald A, 2019 A simulation framework for benchmarking EEG-based brain connectivity estimation methodologies. Brain Topogr 32, 625–642. 10.1007/s10548-016-0498-y. [PubMed: 27255482]

He W, Sowman PF, Brock J, Etchell AC, Stam CJ, Hillebrand A, 2019 Increased segregation of functional networks in developing brains. Neuroimage 200, 607–620. 10.1016/j.neuroimage.2019.06.055. [PubMed: 31271847]

Hiltunen T, Kantola J, Abou Elseoud A, Lepola P, Suominen K, Starck T, Nikkinen J, Remes J, Tervonen O, Palva S, Kiviniemi V, Palva JM, 2014 Infra-slow EEG fluctuations are correlated with resting-state network dynamics in fMRI. J. Neurosci 34, 356–362. 10.1523/JNEUROSCI.0276-13.2014. [PubMed: 24403137]

Hipp JF, Siegel M, 2015 BOLD fMRI correlation reflects frequency-specific neuronal correlation. Curr. Biol 25, 1368–1374. 10.1016/j.cub.2015.03.049. [PubMed: 25936551]

Ilin A, Raiko T, 2010 Practical approaches to principal component analysis in the presence of missing values. J. Mach. Learn. Res 11, 1957–2000.

Ingalhalikar M, Smith A, Parker D, Satterthwaite TD, Elliott MA, Ruparel K, Hakonarson H, Gur RE, Gur RC, Verma R, 2014 Sex differences in the structural connectome of the human brain. Proc. Natl. Acad. Sci 111, 823–828. 10.1073/pnas.1316909110. [PubMed: 24297904]

Keller CJ, Bickel S, Honey CJ, Groppe DM, Entz L, Craddock RC, Lado FA, Kelly C, Milham M, Mehta AD, 2013 Neurophysiological investigation of spontaneous correlated and anticorrelated fluctuations of the BOLD signal. J. Neurosci 33, 6333–6342. 10.1523/JNEUROSCI.4837-12.2013. [PubMed: 23575832]

Kilpatrick LA, Zald DH, Pardo JV, Cahill LF, 2006 Sex-related differences in amygdala functional connectivity during resting conditions. Neuroimage 30, 452–461. 10.1016/j.neuroimage.2005.09.065. [PubMed: 16326115]

Kitzbichler MG, Khan S, Ganesan S, Vangel MG, Herbert MR, Hämäläinen MS, Kenet T, 2015 Altered development and multifaceted band-specific abnormalities of resting state networks in

autism. Biol. Psychiatr. Autism Genotypes and Phenotypes 77, 794–804. 10.1016/j.biopsych.2014.05.012.

Kitzbichler MG, Smith ML, Christensen SR, Bullmore E, 2009 Broadband criticality of human brain network synchronization. PLoS Comput. Biol 5, e1000314 10.1371/journal.pcbi.1000314. [PubMed: 19300473]

Kybic J, Clerc M, Abboud T, Faugeras O, Keriven R, Papadopoulo T, 2005 A common formalism for the Integral formulations of the forward EEG problem. IEEE Trans. Med. Imag 24, 12–28. 10.1109/TMI.2004.837363.

Lai M, Demuru M, Hillebrand A, Fraschini M, 2018 A comparison between scalp-and source-reconstructed EEG networks. Sci. Rep 8, 1–8. 10.1038/s41598-018-30869-w. [PubMed: 29311619]

Lashkari D, Vul E, Kanwisher N, Golland P, 2010 Discovering structure in the space of fMRI selectivity profiles. Neuroimage 50, 1085–1098. 10.1016/j.neuroimage.2009.12.106. [PubMed: 20053382]

Laumann TO, Gordon EM, Adeyemo B, Snyder AZ, Joo SJ, Chen M-Y, Gilmore AW, McDermott KB, Nelson SM, Dosenbach NUF, Schlaggar BL, Mumford JA, Poldrack RA, Petersen SE, 2015 Functional system and areal organization of a highly sampled individual human brain. Neuron 87, 657–670. 10.1016/j.neuron.2015.06.037. [PubMed: 26212711]

Lavanga M, Wel OD, Caicedo A, Jansen K, Dereymaeker A, Naulaers G, Huffel SV, 2018 A brain-age model for preterm infants based on functional connectivity. Physiol. Meas 39, 044006 10.1088/1361-6579/aabac4. [PubMed: 29596059]

Liu Q, Farahibozorg S, Porcaro C, Wenderoth N, Mantini D, 2017 Detecting large-scale networks in the human brain using high-density electroencephalography: imaging Brain Networks with High Density EEG. Hum. Brain Mapp 38, 4631–4643. 10.1002/hbm.23688. [PubMed: 28631281]

Liu Q, Ganzetti M, Wenderoth N, Mantini D, 2018 Detecting large-scale brain networks using EEG: impact of electrode density, head modeling and source localization. Front. Neuroinf 12, 4 10.3389/fninf.2018.00004.

Lock EF, Hoadley KA, Marron JS, Nobel AB, 2013 Joint and individual variation explained (JIVE) for integrated analysis of multiple data types. Ann. Appl. Stat 7, 523–542. 10.1214/12-AOAS597. [PubMed: 23745156]

Logothetis NK, Pauls J, Augath M, Trinath T, Oeltermann A, 2001 Neurophysiological investigation of the basis of the fMRI signal. Nature 412, 150–157. 10.1038/35084005. [PubMed: 11449264]

Madsen J, Margulis EH, Simchy-Gross R, Parra LC, 2019 Music synchronizes brainwaves across listeners with strong effects of repetition, familiarity and training. Sci. Rep 9, 3576 10.1038/s41598-019-40254-w. [PubMed: 30837633]

Mahjoory K, Nikulin VV, Botrel L, Linkenkaer-Hansen K, Fato MM, Haufe S, 2017 Consistency of EEG source localization and connectivity estimates. Neuroimage 152, 590–601. 10.1016/j.neuroimage.2017.02.076. [PubMed: 28300640]

Marzetti L, Basti A, Chella F, D'Andrea A, Syrjälä J, Pizzella V, 2019 Brain functional connectivity through phase coupling of neuronal oscillations: a perspective from magnetoencephalography. Front. Neurosci. Lausanne 13 10.3389/fnins.2019.00964.

Mcardle BH, Anderson MJ, 2001 Fitting multivariate models to community data: a comment on distance-based redundancy analysis, 82, 8.

McGraw KO, Wong SP, 1996 Forming inferences about some intraclass correlation coefficients. Psychol. Methods 1, 30–46. 10.1037/1082-989X.1.1.30.

Meunier D, Achard S, Morcom A, Bullmore E, 2009 Age-related changes in modular organization of human brain functional networks. Neuroimage 44, 715–723. 10.1016/j.neuroimage.2008.09.062. [PubMed: 19027073]

Mowinckel AM, Espeseth T, Westlye LT, 2012 Network-specific effects of age and in-scanner subject motion: a resting-state fMRI study of 238 healthy adults. Neuroimage 63, 1364–1373. 10.1016/j.neuroimage.2012.08.004. [PubMed: 22992492]

Muthukumaraswamy S, 2013 High-frequency brain activity and muscle artifacts in MEG/EEG: a review and recommendations. Front. Hum. Neurosci 7 10.3389/fnhum.2013.00138.

Noble S, Scheinost D, Constable RT, 2019 A decade of test-retest reliability of functional connectivity: a systematic review and meta-analysis. Neuroimage 116157 10.1016/j.neuroimage.2019.116157.

Nolte G, Bai O, Wheaton L, Mari Z, Vorbach S, Hallett M, 2004 Identifying true brain interaction from EEG data using the imaginary part of coherency. Clin. Neurophysiol 115, 2292–2307. 10.1016/j.clinph.2004.04.029. [PubMed: 15351371]

Nolte G, Galindo-Leon E, Li Z, Liu X, Engel AK, 2019 Mathematical relations between measures of brain connectivity estimated from electrophysiological recordings for Gaussian distributed data (preprint). bioRxiv 10.1101/680678. Submitted for publication.

Nunez PL, Srinivasan R, 2016 Electric Fields of the Brain: the Neurophysics of EEG, Electric Fields of the Brain Oxford University Press.

O'Connor D, Potler NV, Kovacs M, Xu T, Ai L, Pellman J, Vanderwal T, Parra LC, Cohen S, Ghosh S, Escalera J, Grant-Villegas N, Osman Y, Bui A, Craddock RC, Milham MP, 2017 The Healthy Brain Network Serial Scanning Initiative: a resource for evaluating inter-individual differences and their reliabilities across scan conditions and sessions. GigaScience 6 10.1093/gigascience/giw011.

Oostenveld R, Fries P, Maris E, Schoffelen J-M, 2011 FieldTrip: open source software for advanced analysis of MEG, EEG, and invasive electrophysiological data. Comput. Intell. Neurosci 1–9 10.1155/2011/156869,2011.

Palva JM, Wang SH, Palva S, Zhigalov A, Monto S, Brookes MJ, Schoffelen JM, Jerbi K, 2018 Ghost interactions in MEG/EEG source space: a note of caution on inter-areal coupling measures. Neuroimage 173, 632–643. 10.1016/j.neuroimage.2018.02.032. [PubMed: 29477441]

Parra LC, Spence CD, Gerson AD, Sajda P, 2005 Recipes for the linear analysis of EEG. Neuroimage 28, 326–341. 10.1016/j.neuroimage.2005.05.032. [PubMed: 16084117]

Pascual-Marqui RD, 2007 Discrete, 3D Distributed, Linear Imaging Methods of Electric Neuronal Activity. Part 1: Exact, Zero Error Localization. ArXiv07103341 Math-Ph Physicsphysics Q-Bio

Pascual-Marqui RD, Lehmann D, Koukkou M, Kochi K, Anderer P, Saletu B, Tanaka H, Hirata K, John ER, Prichep L, Biscay-Lirio R, Kinoshita T, 2011 Assessing interactions in the brain with exact low-resolution electromagnetic tomography. Philos. Trans. R. Soc. Math. Phys. Eng. Sci 369, 3768–3784. 10.1098/rsta.2011.0081.

Pasquale F. de, Penna SD, Snyder AZ, Lewis C, Mantini D, Marzetti L, Belardinelli P, Ciancetta L, Pizzella V, Romani GL, Corbetta M, 2010 Temporal dynamics of spontaneous MEG activity in brain networks. Proc. Natl. Acad. Sci 107, 6040–6045. 10.1073/pnas.0913863107. [PubMed: 20304792]

Patriat R, Molloy EK, Meier TB, Kirk GR, Nair VA, Meyerand ME, Prabhakaran V, Birn RM, 2013 The effect of resting condition on resting-state fMRI reliability and consistency: a comparison between resting with eyes open, closed, and fixated. Neuroimage 78, 463–473. 10.1016/j.neuroimage.2013.04.013. [PubMed: 23597935]

Reid AT, Headley DB, Mill RD, Sanchez-Romero R, Uddin LQ, Marinazzo D, Lurie DJ, Valdés-Sosa PA, Hanson SJ, Biswal BB, Calhoun V, Poldrack RA, Cole MW, 2019 Advancing functional connectivity research from association to causation. Nat. Neurosci 1–10 10.1038/s41593-019-0510-4. [PubMed: 30559474]

Reiss PT, Stevens MHH, Shehzad Z, Petkova E, Milham MP, 2010 On distance-based permutation tests for between-group comparisons. Biometrics 66, 636–643. 10.1111/j.1541-0420.2009.01300.x. [PubMed: 19673867]

Repovš Grega, 2010 Dealing with noise in EEG recording and data analysis. Inf. Med. Slov 15, 18–25.

Rosenberg MD, Finn ES, Scheinost D, Papademetris X, Shen X, Constable RT, Chun MM, 2016 A neuromarker of sustained attention from whole-brain functional connectivity. Nat. Neurosci 19, 165–171. 10.1038/nn.4179. [PubMed: 26595653]

Roweis S, 1998 EM algorithms for PCA and SPCA. Adv. Neural Inf. Process. Syst 626–632.

Salvador R, Suckling J, Schwarzbauer C, Bullmore E, 2005 Undirected graphs of frequency-dependent functional connectivity in whole brain networks. Philos. Trans. R. Soc. B Biol. Sci 360, 937–946. 10.1098/rstb.2005.1645.

Schaefer A, Kong R, Gordon EM, Laumann TO, Zuo X-N, Holmes AJ, Eickhoff SB, Yeo BTT, 2018 Local-global parcellation of the human cerebral cortex from intrinsic functional connectivity MRI. Cerebr. Cortex 28, 3095–3114. 10.1093/cercor/bhx179.

Schäfer CB, Morgan BR, Ye AX, Taylor MJ, Doesburg SM, 2014 Oscillations, networks, and their development: MEG connectivity changes with age. Hum. Brain Mapp 35, 5249–5261. 10.1002/hbm.22547. [PubMed: 24861830]

Schmälzle R, Imhof MA, Grall C, Flaisch T, Schupp HT, 2017 Reliability of fMRI time series: similarity of neural processing during movie viewing (preprint). bioRxiv 10.1101/158188.

Shehzad Z, Kelly C, Reiss PT, Cameron Craddock R, Emerson JW, McMahon K, Copland DA, Xavier Castellanos F, Milham MP, 2014 A multivariate distance-based analytic framework for connectome-wide association studies. Neuroimage 93, 74–94. 10.1016/j.neuroimage.2014.02.024. [PubMed: 24583255]

Shen C, Priebe CE, Vogelstein JT, 2018 From distance correlation to Multiscale graph correlation. J. Am. Stat. Assoc 1–22 10.1080/01621459.2018.1543125. [PubMed: 30034060]

Shou H, Eloyan A, Lee S, Zipunnikov V, Crainiceanu AN, Nebel MB, Caffo B, Lindquist MA, Crainiceanu CM, 2013 Quantifying the reliability of image replication studies: the image intraclass correlation coefficient (I2C2). Cognit. Affect Behav. Neurosci 13, 714–724. 10.3758/s13415-013-0196-0. [PubMed: 24022791]

Shrout PE, Fleiss JL, 1979 Intraclass correlations: uses in assessing rater reliability. Psychol. Bull 86, 420–428. 10.1037/0033-2909.86.2.420. [PubMed: 18839484]

Siems M, Siegel M, 2020 Dissociated neuronal phase- and amplitude-coupling patterns in the human brain. Neuroimage 209, 116538 10.1016/j.neuroimage.2020.116538. [PubMed: 31935522]

Simard I, Luck D, Mottron L, Zeffiro TA, Souli eres I, 2015 Autistic fluid intelligence: increased reliance on visual functional connectivity with diminished modulation of coupling by task difficulty. NeuroImage Clin 9, 467–478. 10.1016/j.nicl.2015.09.007. [PubMed: 26594629]

Smith SM, Miller KL, Salimi-Khorshidi G, Webster M, Beckmann CF, Nichols TE, Ramsey JD, Woolrich MW, 2011 Network modelling methods for FMRI. Neuroimage 54, 875–891. 10.1016/j.neuroimage.2010.08.063. [PubMed: 20817103]

Smith SM, Nichols TE, Vidaurre D, Winkler AM, Behrens TEJ, Glasser MF, Ugurbil K, Barch DM, Van Essen DC, Miller KL, 2015 A positive-negative mode of population covariation links brain connectivity, demographics and behavior. Nat. Neurosci 18, 1565–1567. 10.1038/nn.4125. [PubMed: 26414616]

Sudre G, Szekely E, Sharp W, Kasparek S, Shaw P, 2017 Multimodal mapping of the brain's functional connectivity and the adult outcome of attention deficit hyperactivity disorder. Proc. Natl. Acad. Sci 114, 11787–11792. 10.1073/pnas.1705229114. [PubMed: 29078281]

Tadel F, Baillet S, Mosher JC, Pantazis D, Leahy RM, 2011 Brainstorm: a user-friendly application for MEG/EEG analysis. Comput. Intell. Neurosci 2011, 1–13. 10.1155/2011/879716. [PubMed: 21837235]

Takagi Y, Hirayama J, Tanaka SC, 2019 State-unspecific patterns of whole-brain functional connectivity from resting and multiple task states predict stable individual traits. Neuroimage 201, 116036 10.1016/j.neuroimage.2019.116036. [PubMed: 31326571]

Tomasi D, Volkow ND, 2012 Gender differences in brain functional connectivity density. Hum. Brain Mapp 33, 849–860. 10.1002/hbm.21252. [PubMed: 21425398]

Turkheimer E, Haley A, Waldron M, D'Onofrio B, Gottesman II, 2003 Socioeconomic status modifies heritability of IQ in young children. Psychol. Sci 14, 623–628. 10.1046/j.0956-7976.2003.psci_1475.x. [PubMed: 14629696]

Vanderwal T, Eilbott J, Finn ES, Craddock RC, Turnbull A, Castellanos FX, 2017 Individual differences in functional connectivity during naturalistic viewing conditions. Neuroimage 157, 521–530. 10.1016/j.neuroimage.2017.06.027. [PubMed: 28625875]

Vanegas MI, Blangero A, Kelly SP, 2015 Electrophysiological indices of surround suppression in humans. J. Neurophysiol 113, 1100–1109. 10.1152/jn.00774.2014. [PubMed: 25411464]

Venkatesh M, Jaja J, Pessoa L, 2020 Comparing functional connectivity matrices: a geometry-aware approach applied to participant identification. Neuroimage 207, 116398 10.1016/j.neuroimage.2019.116398. [PubMed: 31783117]

Vogelstein JT, Bridgeford EW, Wang Q, Priebe CE, Maggioni M, Shen C, 2019 Discovering and deciphering relationships across disparate data modalities. eLife 8, e41690 10.7554/eLife.41690. [PubMed: 30644820]

Wang HE, B enar CG, Quilichini PP, Friston KJ, Jirsa VK, Bernard C, 2014 A systematic framework for functional connectivity measures. Front. Neurosci 8 10.3389/fnins.2014.00405.

Wang J, Ren Y, Hu X, Nguyen VT, Guo L, Han J, Guo CC, 2017 Test-retest reliability of functional connectivity networks during naturalistic fMRI paradigms: test-Retest Reliability of Naturalistic fMRI. Hum. Brain Mapp 38, 2226–2241. 10.1002/hbm.23517. [PubMed: 28094464]

Wang SH, Lobier M, Siebenhühner F, Puoliväli T, Palva S, Palva JM, 2018 Hyperedge bundling: a practical solution to spurious interactions in MEG/EEG source connectivity analyses. Neuroimage 173, 610–622. 10.1016/j.neuroimage.2018.01.056. [PubMed: 29378318]

Wirsich J, Amico E, Giraud A-L, Goñi J, Sadaghiani S, 2020 Multi-timescale hybrid components of the functional brain connectome: A bimodal EEG-fMRI decomposition. Network Neuroscience 10.1162/netn_a_00135. In press.

Wirsich J, Ridley B, Besson P, Jirsa V, B enar C, Ranjeva J-P, Guye M, 2017 Complementary contributions of concurrent EEG and fMRI connectivity for predicting structural connectivity. Neuroimage 161, 251–260. 10.1016/j.neuroimage.2017.08.055. [PubMed: 28842386]

Yeo T, Krienen FM, Sepulcre J, Sabuncu MR, Lashkari D, Hollinshead M, Roffman JL, Smoller JW, Zöllei L, Polimeni JR, Fischl B, Liu H, Buckner RL, 2011 The organization of the human cerebral cortex estimated by intrinsic functional connectivity. J. Neurophysiol 106, 1125–1165. 10.1152/jn.00338.2011. [PubMed: 21653723]

Yu Q, Risk BB, Zhang K, Marron JS, 2017 JIVE integration of imaging and behavioral data. Neuroimage 152, 38–49. 10.1016/j.neuroimage.2017.02.072. [PubMed: 28246033]

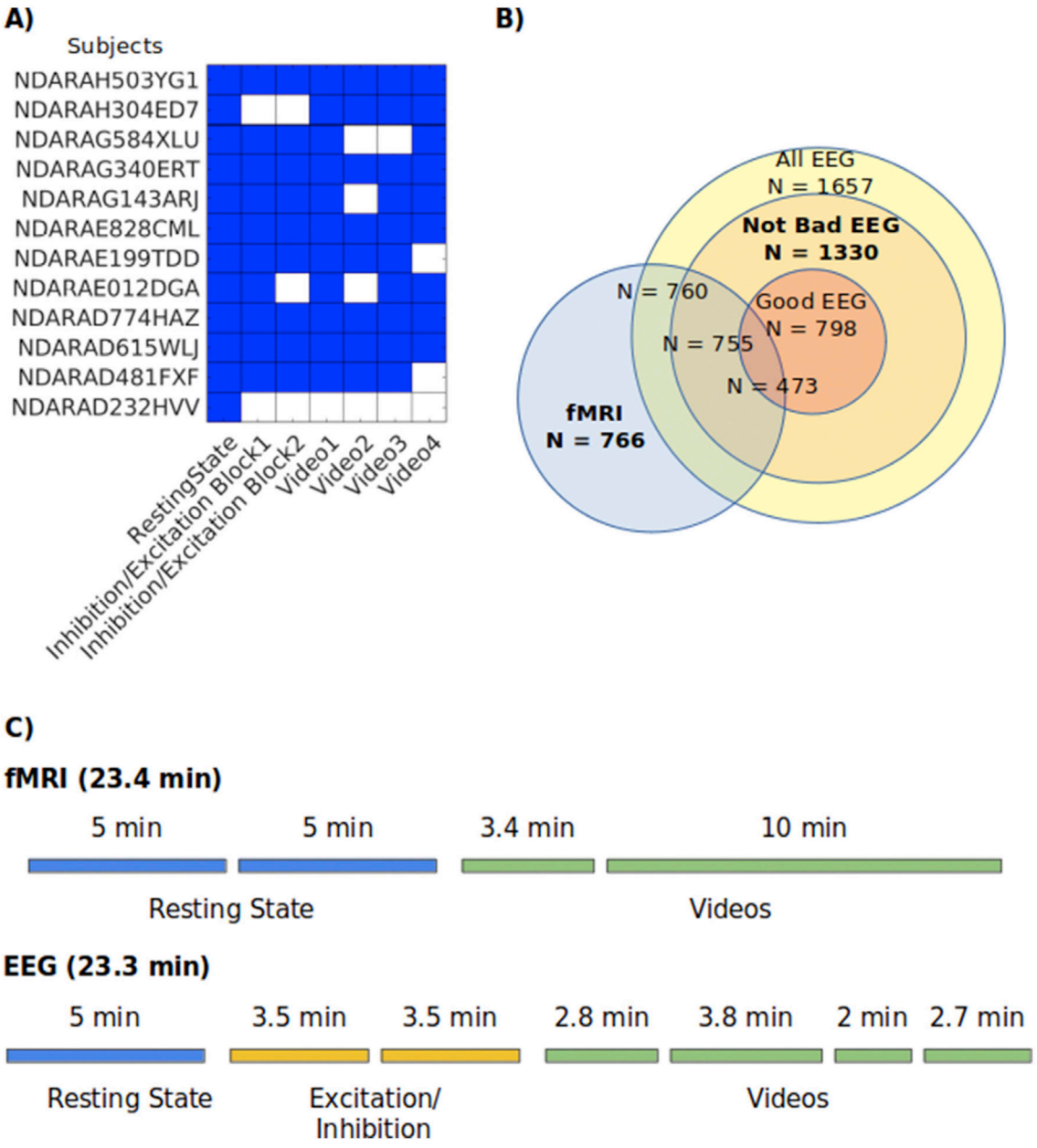

Fig. 1. Data availability.

A) For each subject only tasks that are available on the HBN Biobank and have a reasonable data quality (rating > 4) are concatenated. B) Number of subjects available for each level of data quality, 'All EEG': rating >3, 'Not Bad EEG': rating >4, 'Good EEG': rating = 5; Video 1: 'Diary of a Wimpy Kid', Video 2: 'Fun with Fractals', Video 3: 'Despicable Me', Video 4: 'The Present'; C) Time of recordings per modality and task Ratings of data quality are described in section 5.5.

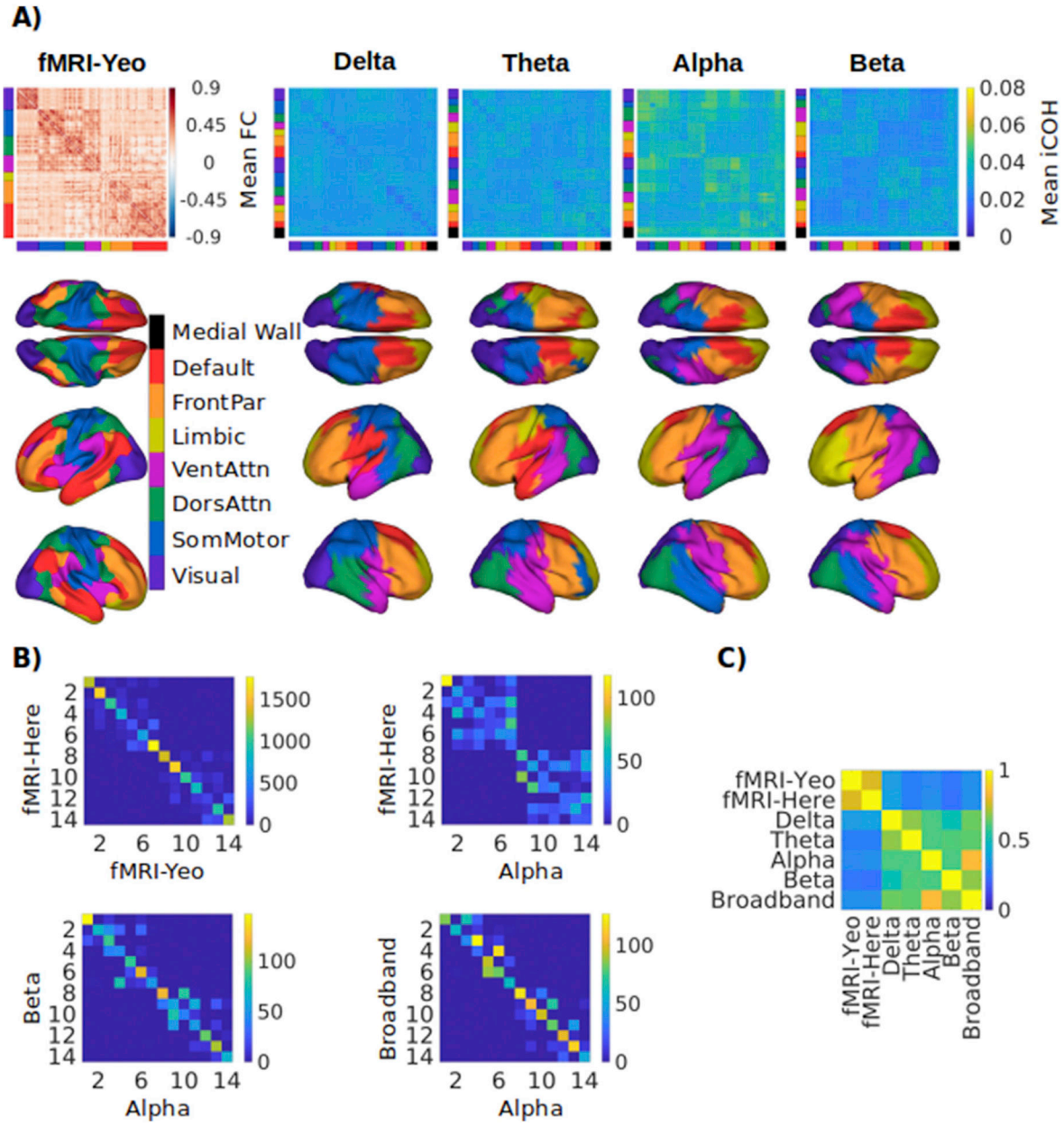

Fig. 2. Clusters in the FC of fMRI and EEG for different frequency bands.

A) Top row shows the mean cortical fMRI connectivity matrix measured as Pearson's correlations, as well as the EEG source space FC matrices measured as iCOH. Here FC is computed with combined data from resting state, naturalistic viewing and a visual stimulation task and averaged over all subjects (fMRI N = 770, EEG: N = 1330). The significance of the connections is reported in Fig. A1. The leftmost column of spatial patterns shows the clusters identified by Yeo et al. (Yeo et al., 2011) in fMRI data based on 200 parcels in the Schafer atlas (Schaefer et al., 2018). Using the EEG data in different bands, connectivity has been clustered using the same analysis conducted by Yeo et al. (Yeo et al., 2011). The corresponding spatial location of the clusters are shown below the connectivity matrices. The colorbars to the left and bottom of the connectivity matrices

indicate the cluster assignment. Broadband FC is most similar to the alpha band and is omitted for brevity. Clusters of the EEG FC have been colored to match the areas in the Yeo atlas with largest overlap, but do not necessarily share the same functions. B) Individual confusion matrices comparing the clustering between different bands and modalities. Values on the diagonal depict the number of voxels assigned to the same clusters. Values on the off-diagonal depict the number of voxels assigned to different clusters in each modality. The colorbar codes for the number of voxels that are in the same or different clusters. C) Similarity of clustering of FC in different EEG frequency bands and modalities measured as the precision of the confusion matrix. The colorbar codes the ratio of voxels assigned to the same cluster over the total number of voxels. Clusters 1–7 are located on the left hemisphere, clusters 8–14 are located on the right hemisphere. ‘fMRI-Yeo’: Clusters defined in Yeo et al. (2011) (Yeo et al., 2011), ‘fMRI-Here’: Clusters defined on fMRI data from the HBN dataset. Resting state and video task data have been concatenated. Cluster 1/8 = Visual; Cluster 2/9 = ‘SomMotor’: Somatomotor; Cluster 3/10 = ‘DorsAttn’: Dorsal Attention; Cluster 4/11 = ‘VentAttn’: Ventral Attention; Cluster 5/12 = Limbic; Cluster 6/13 = ‘FrontPar’: Frontoparietal; Cluster 7/14 = Default.

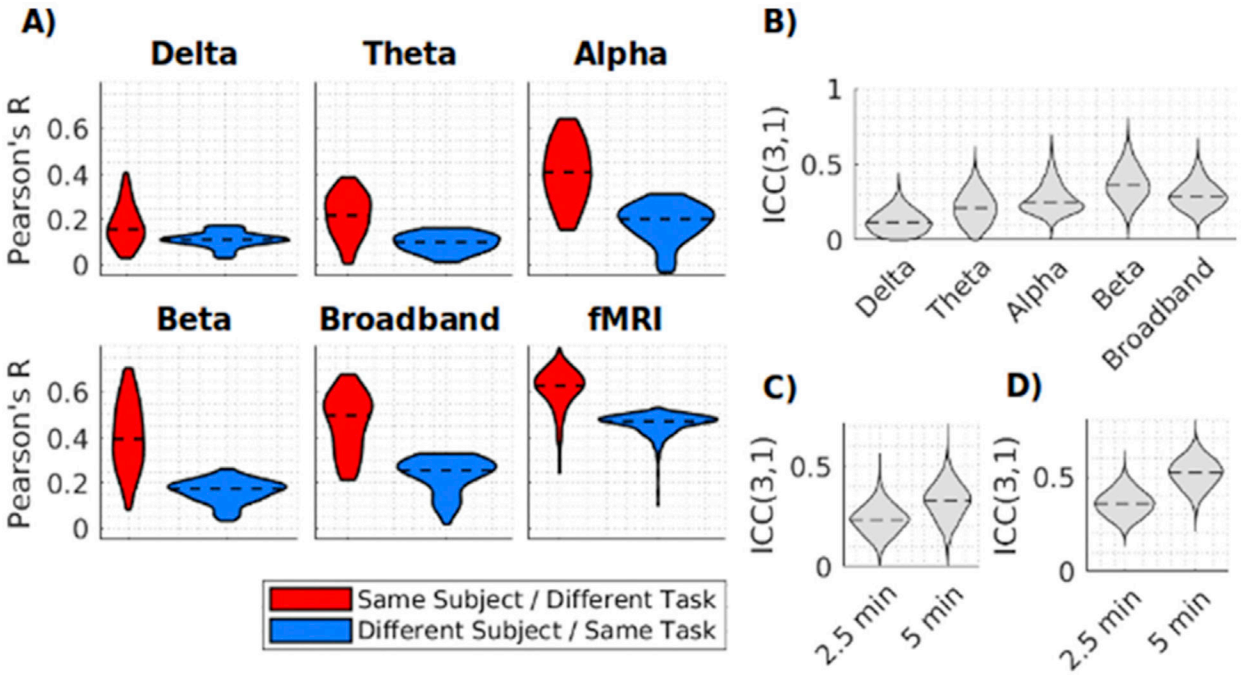

Fig. 3. FC for subjects engaged in different tasks is more similar than for different subjects engaged in the same task.

A) Violin plots depict the distribution of the Pearson's correlation between FC (iCOH) matrices across subjects. Dashed lines indicate the median of the distributions. Pearson's R for 'Same Subject/Different Task' measures the similarity between different tasks (resting state, videos viewing, flashing gradings) computed for each subject separately. Pearson's R for 'Different Subject/Same Task' measures the similarity between different subjects completing the same task. The correlation values between different subjects in the same task have been averaged per subject across all possible subject pairs. Then, the correlation coefficients from different tasks have been averaged. B) ICC measures reliability across tasks relative to variability across subjects. Distribution of ICC of FC (iCOH) between each pair of brain regions in the Schaefer atlas. We compare connectivity matrices between three tasks (videos, resting state and inhibition/excitation paradigm). The distribution of ICC is displayed for connectivity in each frequency band. Corresponding matrices are shown in Fig. A2. C) Distribution of ICC of FC between brain areas in resting state increases with length of recording time. ICC is computed between connectivity matrices of different sessions. Dashed lines show the median of the distributions. Median difference of ICC between 2.5 and 5 min sessions: $\Delta_r = 0.094$, $p \approx 0$. Matrices of ICC for all pairs of regions are shown in Fig. A3A. D) ICC of FC during a video task (10 min of 'Despicable Me') increases with recording time. ICC is computed between sessions of the same movie task. Median difference of ICC between 2.5 and 5 min sessions: $\Delta_r = 0.16$, $p \approx 0$. Corresponding matrices of reliability are shown in Fig. A3B.

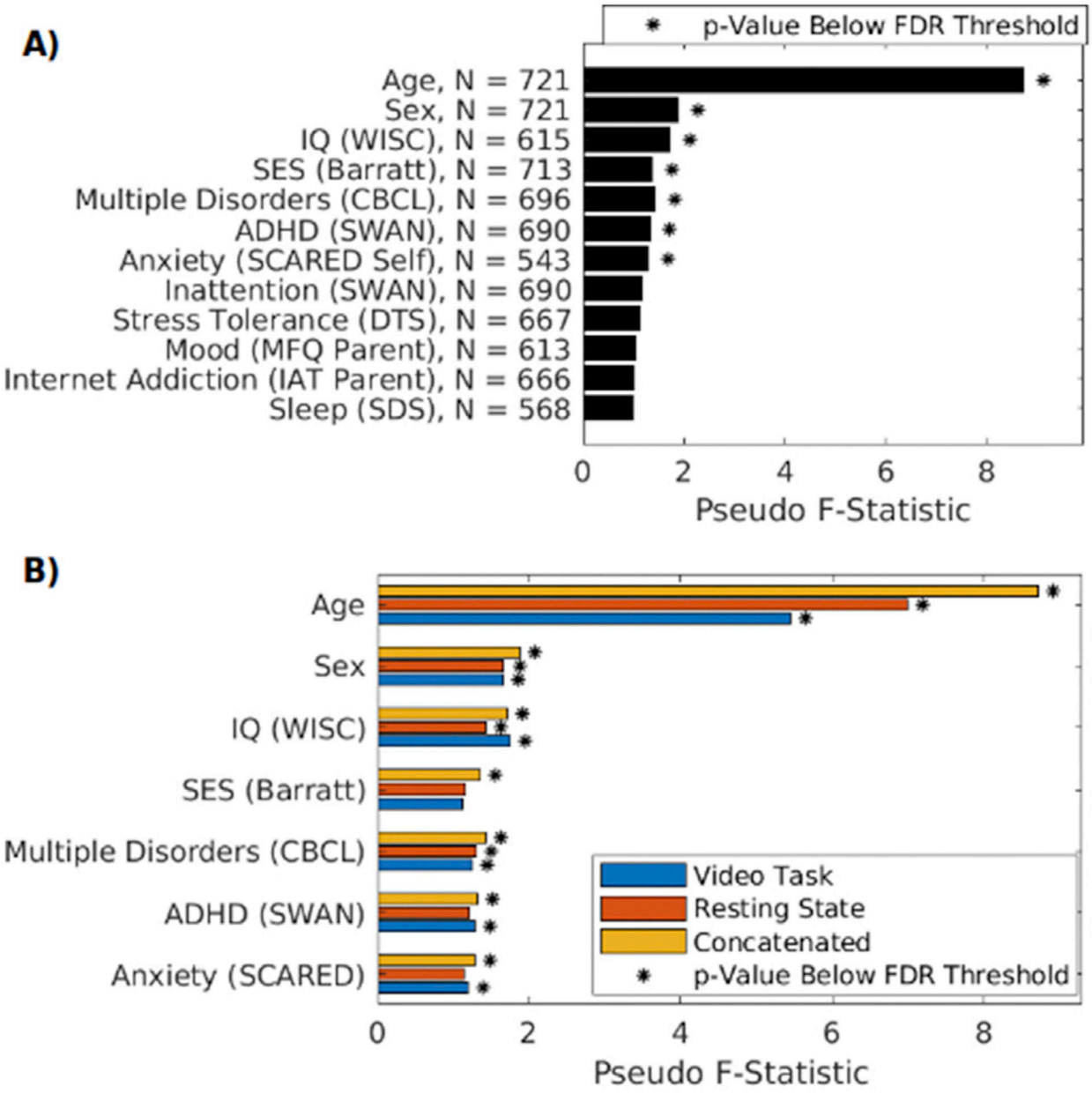

Fig. 4. fMRI FC correlates with demographic and phenotypic measures.

MDMR analysis was performed for each demographic/phenotype information separately. The Pseudo F-Statistic measures how much of the total variance of the similarity of subjects can be explained by demographic/phenotype information. A) Results of the MDMR analysis using concatenated fMRI data and showing all phenotypes tested. Numbers indicate number of individuals for which fMRI of sufficient quality and specific demographic/phenotype information was available. B) Connectivity-phenotype relationship computed separately with data from each task. Sex: biological sex. Phenotypes not shown are not significantly related to connectivity in any task. SWAN: Strengths and Weaknesses of Attention-Deficit Hyperactivity-symptoms and Normal-behaviors. WISC: Wechsler Intelligence Scale for Children. Barratt: Barratt Simplified Measure of Social Status. IAT Parent: Internet

Addiction Test assessed by a parent. CBCL: Child Behavior Checklist. MFQ Patent: Mood and Feelings Questionnaire assessed by a parent. SCARED self: Screen for Child Anxiety Related Disorders assessed by the minor. SDS: Sleep Disturbance Scale assessed by a parent. DTS: Distress Tolerance Scale. False discovery rate (FDR) control, at a level of $\alpha = 0.05$, was performed over the 12 variables tested here.

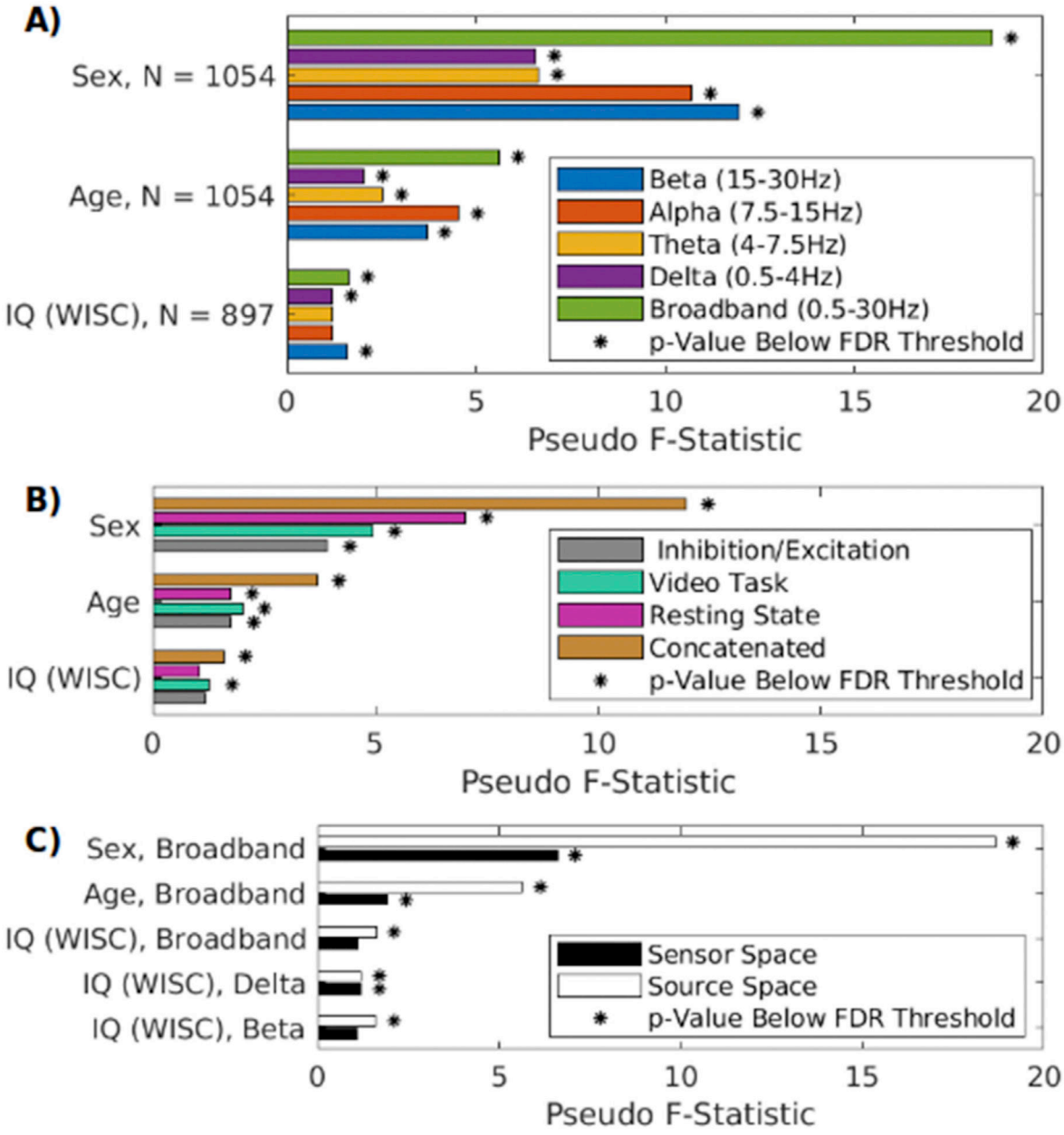

Fig. 5. EEG FC in various frequency bands are associated to sex, age and IQ.

A) FC (iCOH) was computed after source localization. FDR correction was performed here across 12 measures (the same as in Fig. 4A), but not across bands. The 9 phenotypes not shown here, but shown in Fig. 4A, had no significant association with EEG FC in any frequency band. B) FC of EEG (source space, beta band) is associated with phenotype when FC is computed separately for each task C) The FC-phenotype association is stronger when FC is computed in source space as opposed to sensor space. Sex and age effect are shown for one frequency band as and example. Effects of IQ are shown for all bands that show a significant effect in either source or sensor space. The effect for sex and age is present for all other frequency bands (Fig. A8). FDR control, at a level of $\alpha = 0.05$, was performed over the 12 variables tested here.

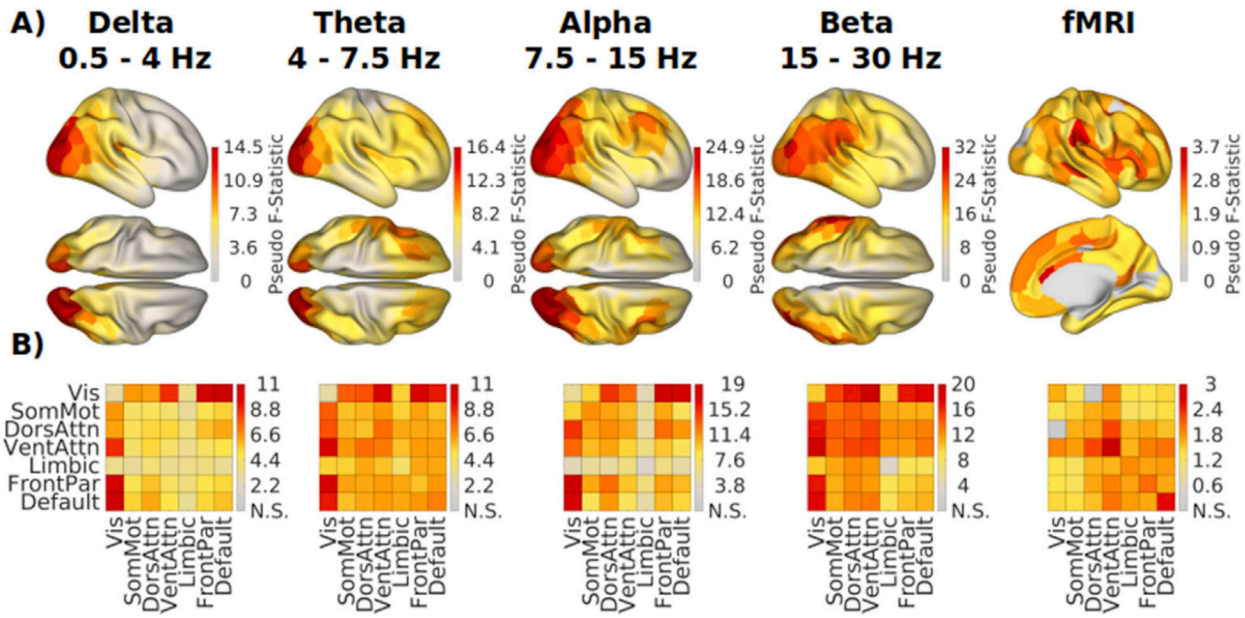

Fig. 6. Functional connections with significant sex effect.

A) Spatial pattern of connectivity - sex relationship in EEG source space and fMRI. The subject-by-subject distance matrix is computed for each brain region. The distance is the Pearson's correlation between the vectors of connectivity for each region. Pseudo F-Statistic for EEG and fMRI connectivity - sex association is computed by MDMR (Shehzad et al., 2014). Significant pseudo F-statistic values are plotted on the surface of the Freesurfer fsaverage template after correcting for multiple comparisons (FDR correction at $\alpha = 0.05$). A high pseudo F-statistic in a brain region indicates that between-subject differences in connectivity patterns to all other regions correspond to differences in sex. B) Pseudo F-Statistic for the relationship between sex and the connectivity patterns in resting state networks of the Yeo parcellation (Schaefer et al., 2018; Yeo et al., 2011). Each square depicts the strength of the relationship of sex and the connectivity within (diagonal) or between (off-diagonal) networks. FDR correction at $\alpha = 0.05$ was performed. Vis: Visual, SomMot: Somatomotor, DorsAttn: Dorsal Attention, VentAttn: Ventral Attention, FrontPar: Frontoparietal.

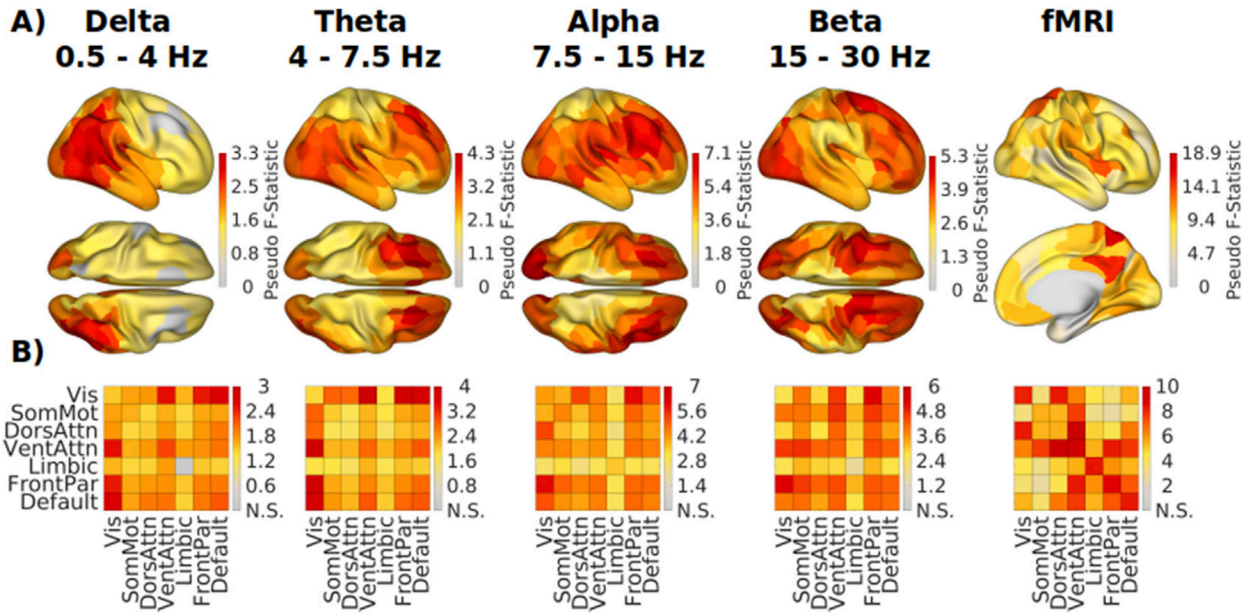

Fig. 7. Functional connections with significant age effect.

A) Spatially resolved EEG source space and fMRI FC - age association based on each Schaefer brain region as a seed. B) Relationship of connectivity in resting state networks to age. Correction for multiple comparisons as in Fig. 6.

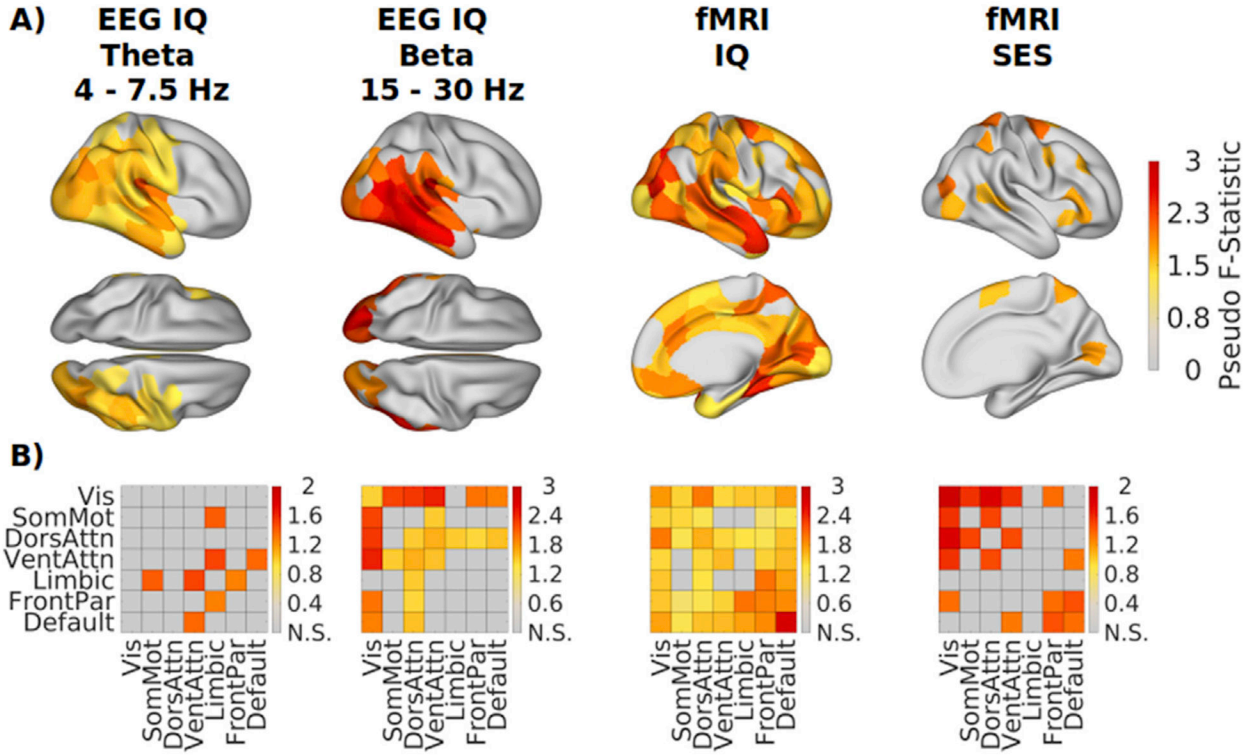

Fig. 8. EEG functional connections with significant effects of phenotypes.

A) EEG source space and fMRI FC - phenotype (IQ and SES) association based on each Schaefer brain region as a seed. B) Relationship of connectivity in resting state networks to IQ and SES. Correction for multiple comparisons as in Fig. 6.

Table 1

Percentile threshold used to assign data quality ratings.

Lower Percentile	Upper Percentile	Rating
	30	5
30	60	4
60	90	3
90	99	2
99		1